2 Birefringent Optical Waveguides

María L. Calvo and Ramón F. Alvarez-Estrada

CONTENTS

2.1 INTRODUCTION

At the macroscopic scale (the one considered throughout this article), a dielectric material is optically isotropic if, at any given spatial location in it, its optical properties are the same for any direction.[1–3] Then, at a given spatial location in that medium, there is only one dielectric permittivity (for a given frequency of light) and, hence, only one refractive index of light. Gases, liquids and amorphous solids constitute relevant optically isotropic dielectric materials (in particular, glass is a remarkably important example of such an amorphous solid). Various general and specific aspects of the propagation and scattering of the electromagnetic field in optically isotropic materials are, by now, well understood and are well documented.[2,4–7]

Several decades ago, the confined propagation of light was achieved experimentally in optically isotropic dielectric fibers (optical fibers), namely, thin solid waveguides with transverse dimensions about tens of wavelengths. Optical fibers, with transverse sizes in the micron range, have had great technological impact. Very interesting physics in that confined propagation lies in the fact that the electromagnetic wave aspects of light have to be taken into account (say, a geometrical–optics formulation, although very useful, does not describe various important features). Thus, light is transmitted along the fiber only in the form of some specific distributions of the electromagnetic field (solving Maxwell's equations), named propagation modes.

Confined propagation of light in optically isotropic fibers has been studied in detail in a number of articles and books.[8–15] Similar and very important phenomena occur in the eye, namely the propagation of light along the retinal photoreceptors, regarded as biological waveguides (the transverse dimensions of which are only a few wavelengths).[16,17] Various aspects of confined propagation of light are also well documented, in an updated way, in different chapters of this book.

Back to optical fibers, it is a fact that the preservation of the polarization state of light, propagating confined along them, is indispensable for their efficient use in coherent optical transmission, for polarization sensitive sensors and for connections with integrated optical waveguide devices.[18] The last fact has stimulated many developments by a large number of researchers, some of which will be summarized succinctly in the present chapter.

On the other hand, an optically anisotropic dielectric material is, by definition, one in which, for a given macroscopically small volume element, the optical properties depend on the chosen direction (also, for a given frequency of light).[1–3] Then, the dielectric permittivity becomes a 3×3 symmetric tensor and there are more than one refractive indices of light (birefringence). This fact implies different and important optical phenomena. The description of the electromagnetic field of light propagating through an optically anisotropic medium is more complicated than that for an isotropic one. Crystals and liquid crystals provide important different classes of optically anisotropic media. Besides crystals and liquid crystals, at least other two important classes of optically anisotropic dielectric materials exist, namely, those due to form birefringence[1] and to the photo-elastic effect (or stress birefringence).[1–3]

The confined propagation of light in optically anisotropic dielectric waveguides is another interesting phenomenon (which, as we shall see, has also become important in the last two decades). It had already attracted attention at some earlier stage.[10,18,19] One motivation for that interest has been the technological importance of preserving, as much as possible, the polarization of the propagation modes subject to various perturbations in optical fibers, as commented above. Thus, it appeared that optically anisotropic dielectric waveguides, due (in particular, but not exclusively, to the photo-elastic effect) could offer some interesting possibilities aimed towards retaining a high degree of polarization, thereby improving optical devices.[18]

On the other hand, by analyzing the scattering of light by a system displaying the photo-elastic effect, one could obtain useful information about that system (say, the stresses in it). Waveguides with induced anisotropy may have additional interest, as they could play a role in biological waveguides (mostly under conditions of pathological functioning), in polarimetric fiber-optic sensors, and in mechanical stress sensors.[20]

We shall comment on those different subjects throughout this chapter. Our emphasis will be essentially methodological. We shall provide some basic descriptions of various systems, in which optical anisotropy arises or could arise. On the other hand, we shall treat certain theoretical foundations of electromagnetic wave scattering by and confined propagation in optically anisotropic systems. Detailed applications of the theoretical formulations to all systems described lie outside our scope. In spite of that, we shall outline some limited applications. We shall refer to the bibliography for specific and additional details.

The contents of the present chapter are the following. Section 2.2 will summarize classical electromagnetic wave propagation in an anisotropic dielectric material. As an introductory example, the propagation of a plane electromagnetic wave in an extended homogeneous anisotropic dielectric medium is discussed briefly in Section 2.2. We overview physically relevant cases in which optical anisotropy occurs in Sections 2.3, 2.4 and 2.5. Section 2.3 outlines it in crystals and liquid crystals. Section 2.4 deals with form birefringence. An account of the photo-elastic effect is given in Section 2.5. Section 2.6 outlines a few aspects of high birefringence in polarimetric optical fibers and sensors. Section 2.7 discusses, rather qualitatively, some aspects of biological waveguides (in the eye) as well as form birefringence in and light scattering by them. Section 2.8 presents a rather general treatment for the scattering of classical electromagnetic radiation by arbitrary three-dimensional optically anisotropic objects, and a multiple-scattering reformulation thereof is outlined in Section 2.9. Section 2.10 deals with scattering by parallel cylindrical dielectric waveguides: one and several waveguides as well as long wavelength approximations are treated. Section 2.11 summarizes recent work on the scattering of light by parallel dielectric waveguides, in which the anisotropy has been generated by the photo-elastic effect, and discusses shortly possible applications to stress sensing. Section 2.12 deals with confined propagation of classical electromagnetic radiation along cylindrical anisotropic dielectric waveguides: in particular, the long wavelength approximation for one waveguide (monomode confined propagation) is analyzed. Section 2.13 contains the conclusions. Various derivations, computations and formulas are collected in several appendixes.

2.2 CLASSICAL ELECTROMAGNETIC WAVES IN ANISOTROPIC DIELECTRIC MEDIA

2.2.1 Maxwell's Equations for Medium

We shall follow the same conventions as Born and Wolf.[1] Let us consider an optically anisotropic dielectric material. The latter has zero electrical conductivity, real scalar magnetic permeability (μ_0) equal to that of vacuum, and a dielectric permittivity tensor given as the product: $\epsilon_0\tilde{\epsilon}$. ϵ_0 is the real constant (scalar) dielectric permittivity of some optically isotropic and homogeneous dielectric reference medium (also with magnetic permeability μ_0), to be discussed later. Then, the constant refractive index of that isotropic reference material is $n_0 = (\epsilon_0\mu_0)^{1/2}$. On the other hand, $\tilde{\epsilon}$ is the dielectric permittivity tensor of the anisotropic material relative to (the permittivity of) the isotropic reference one, mentioned above. $\tilde{\epsilon}$ is a symmetric 3×3 matrix with components ϵ_{ij}, $i, j = 1, 2, 3$ ($\epsilon_{ij} = \epsilon_{ji}$). Each ϵ_{ij} could depend on the three-dimensional spatial position ($\bar{x} = (x_1, x_2, x_3)$) and on the frequency ($\omega$) of a propagating electromagnetic field, and could be either real or complex, in principle. In the general study, we shall allow for ϵ_{ij} to be complex and we shall restrict them to be real, at the appropriate places. If the optically anisotropic medium reduces to an isotropic one, then $\tilde{\epsilon}$ becomes proportional to the 3×3 unit matrix I_3.

Let classical monochromatic (complex) electric ($\mathbf{E}' \exp(-i\omega t)$) and magnetic ($\mathbf{H}' \exp(-i\omega t)$) fields, with real frequency ω, propagate in the anisotropic dielectric medium. As ω will be held fixed, we shall not specify any dependence of ϵ_{ij} on it. The time-dependent factor ($\exp(-i\omega t)$) will always be factored out. The t-independent fields $\mathbf{E}' = \mathbf{E}'(\bar{x})$ and $\mathbf{H}' = \mathbf{H}'(\bar{x})$ fulfill Maxwell's equations for that medium, in the absence of charges:[1]

$$\nabla \times \mathbf{E}' = \frac{i\omega}{v}\left(\frac{\mu_0}{\epsilon_0}\right)^{1/2}\mathbf{H}', \nabla \cdot (\tilde{\epsilon}\mathbf{E}') = 0 \tag{2.1}$$

$$\nabla \times \mathbf{H}' = -\frac{i\omega}{v}\left(\frac{\epsilon_0}{\mu_0}\right)^{1/2}\tilde{\epsilon}\mathbf{E}', \nabla \cdot \mathbf{H}' = 0 \tag{2.2}$$

Here, v denotes the velocity of light in the isotropic reference medium: $v = c/n_0$. c will always denote the velocity of light in vacuum (where $n_0 = 1$).

Let $(\tilde{\epsilon})^{-1}$ denote the (3×3) inverse matrix of $\tilde{\epsilon}$ $((\tilde{\epsilon})^{-1} \cdot \tilde{\epsilon} = I_3$, I_3 being the unit 3×3 matrix). Using $(\tilde{\epsilon})^{-1}$, it is easy to reduce exactly the above system in Eqs. (2.1) and (2.2) involving both $\mathbf{E}'$ and $\mathbf{H}'$ to one system depending only on $\mathbf{H}'$, in which $\mathbf{E}'$ will be eliminated. For that purpose, we perform, successively, the following operations: i) we apply $(\tilde{\epsilon})^{-1}$ to the first equation in Eq. (2.2), ii) we apply $\nabla\times$ to the result of i), iii) in the result of ii), we replace $\nabla \times \mathbf{E}'$ by $(i\omega/v)(\mu_0/\epsilon_0)^{1/2}\mathbf{H}'$. The result is the announced system involving only $\mathbf{H}'$:

$$\nabla \times ((\tilde{\epsilon})^{-1}\nabla \times \mathbf{H}') = \frac{\omega^2}{v^2}\mathbf{H}', \nabla \cdot \mathbf{H}' = 0 \tag{2.3}$$

Clearly, the divergence $(\nabla\cdot)$ of the first equation in Eq. (2.3) is consistent with the second equation in Eq. (2.3). It is also easy to get another system depending only on $\mathbf{E}'$,[10] in which $\mathbf{H}'$ has been eliminated, but we shall not consider it. Our interest in and preference for the first equation in Eq. (2.3) rely upon the fact that $\mathbf{H}'$ is divergenceless, as expressed by the second equation in Eq. (2.3).

Let us now consider two different dielectric media, separated only by a surface Σ (one goes from one medium to the other just by traversing Σ). The boundary conditions to be fulfilled by the electromagnetic field are the following.[1] Across Σ and at any point of it, the following six quantities have to be continuous: i) $\mathbf{H}'$ (its three components), ii) the projection of $\tilde{\epsilon}\mathbf{E}'$ orthogonal to Σ (one quantity), iii) the two tangential components of $\mathbf{E}'$ (namely, the components of the projection of $\mathbf{E}'$ on Σ). In order to simplify the analysis, we shall always suppose that all components of the tensor $\tilde{\epsilon}$ and all their spatial derivatives of first order are continuous inside each dielectric media. At this stage, the behaviors of the components of the tensor $\tilde{\epsilon}$ (and of the derivatives thereof) across the interface Σ separating two different dielectric media have not yet been specified, but we shall have to make suitable assumptions also about them as we proceed. Of course, Eqs. (2.1), (2.2) and (2.3) hold independently on assumptions about $\tilde{\epsilon}$ and their first spatial derivatives across any such interface.

2.2.2 Extended and Homogeneous Anisotropic Medium

As a simple illustration of electromagnetic wave propagation in an anisotropic dielectric medium, we shall suppose that the latter is very extended and has no inhomogeneities, that is, $\tilde{\epsilon}$ is constant ($\bar{x}$-independent) and it is not proportional to I_3. In such a case, we shall choose the three axis x_1, x_2, x_3 of Cartesian coordinates so that they coincide with the principal axis of the symmetric tensor $\tilde{\epsilon}$. That is, with respect to such a coordinate system, $\tilde{\epsilon}$ is represented by a diagonal matrix ($\epsilon_{ij} = 0$, for $i \neq j$). The anisotropic medium is called uniaxial, if two out of the three non-vanishing diagonal elements (eigenvalues) ϵ_{ii} are equal to each other, the third one being different from them. The medium is named biaxial, if all three non-vanishing diagonal values ϵ_{ii} are different from one another.

In such a coordinate system where $\tilde{\epsilon}$ is diagonal, we shall consider the propagation of an electromagnetic plane wave with frequency ω and wavevector $\bar{k} = (k_1, k_2, k_3)$. Such an electromagnetic wave has to be a solution of Eqs. (2.1) and (2.2) (or, equivalently, of Eq. (2.3)) for any $\bar{x}$. Those equations imply an important relationship (the dispersion relation) between $\bar{k}$ and ω. The dispersion relation for an anisotropic dielectric medium is more complicated than (and contains new physical information compared to) that for an isotropic one. The anisotropic dispersion relation is known as the Fresnel equation. We use the known structure of the latter[1] and recast it in terms of $\bar{k}$ and ω. Then, the Fresnel equation reads:

$$\frac{(k_1/\mid \bar{k}\mid)^2}{[v\mid \bar{k}\mid/\omega]^2-\mu_0\epsilon_{11}}+\frac{(k_2/\mid \bar{k}\mid)^2}{[v\mid \bar{k}\mid/\omega]^2-\mu_0\epsilon_{22}}+\frac{(k_3/\mid \bar{k}\mid)^2}{[v\mid \bar{k}\mid/\omega]^2-\mu_0\epsilon_{33}}
=\frac{1}{[v\mid \bar{k}\mid/\omega]^2} \tag{2.4}$$

Various derivations of the Fresnel equation[1–3] employ all Eqs. (2.1) and (2.2). An important physical feature is that, by virtue of anisotropy, the dispersion relation (2.4) has two (but not more) different solutions for ω^2, for a given $\bar{k}$ (birefringence). There is an important physical reason for that (namely, that there are only two independent states of polarization for an electromagnetic plane wave): such a motivation has been succinctly stated,[2] and also explained in more algebraic detail[3] in terms of $\tilde{\epsilon}\mathbf{E}'$ (the displacement vector). In Appendix A, we shall outline that physical reason, based upon $\mathbf{H}'$ and Eq. (2.3) (thereby allowing us to put them to work). Appendix A will employ the standard unit polarization vectors, which will be also useful when dealing with scattering by optically anisotropic objects in three dimensions. We shall not stop to use $\mathbf{H}'$ and Eq. (2.3) in order to provide another algebraic derivation of the Fresnel equation. $\mathbf{H}'$ and (2.3) will turn out to be quite useful for general studies about scattering and confined propagation, later in this chapter.

Below, we shall allow, in principle, for the possibility that $\tilde{\epsilon}$ is not only ω-dependent but $\bar{x}$-dependent as well. We shall study phenomena determined by one or several essentially parallel cylindrical anisotropic dielectric waveguides: wherever possible in those cases, it will certainly be advantageous to choose the x_3-axis so that it is parallel to the axis of the cylindrical waveguides. That x_3-axis will, in principle, be different from any of the principal axes of the symmetric tensor $\tilde{\epsilon}$. Then, $\tilde{\epsilon}$ will not be represented by a diagonal matrix for any $\bar{x}$, in general (although it may be, in some special cases).

2.3 OPTICAL ANISOTROPY(I): CRYSTALS AND LIQUID CRYSTALS

Let us consider a crystal, the size of which is not too small. It is formed by a suitably large number of atoms or molecules, the locations of which form a regular pattern (essentially periodic in the spatial region occupied by the crystal): positional order. The atoms and molecules have essentially fixed and well-defined positions and orientations in the crystal. Moreover, the electrical properties of those atoms and molecules are typically anisotropic. Altogether, those facts imply that, in principle, the properties of the crystal are not the same in all directions, namely, anisotropy.[1]

The propagation of electromagnetic waves (and, in particular, of light) in crystals depends, typically but not necessarily, on the direction. That is, crystals may display, but not necessarily, optical anisotropy. In fact, there are crystals in which the relative dielectric permittivity tensor reduces to a scalar (that is, $\tilde{\epsilon}$ becomes proportional, but not equal, to the 3×3 unit matrix I_3). Such crystals are those belonging to the so-called cubic system (in which three mutually orthogonal and crystallographically equivalent directions may be chosen). Crystals belonging not to the cubic system, but to either the trigonal or the tetragonal or the hexagonal systems (in all of which, two or more crystallographically equivalent directions may be chosen in one plane) are uniaxial and, so, optically anisotropic. Crystals belonging not to any of the above four systems but to either the orthorhombic or the monoclinic or the triclinic systems (in all of which, no two crystallographically equivalent directions may be chosen) are biaxial and, so, optically anisotropic as well. Quartz and calcite are examples of uniaxial crystals. Aragonite and Brazil topaz provide examples of biaxial crystals.

A crystalline grain can be regarded as a crystal, the size of which is quite small. As the number of atoms forming it is not small, and since their spatial locations resemble those for a proper crystal, as outlined above, a crystalline grain may also display, in general, a similar type of optical anisotropy. On the other hand, what one usually meets and handles easily is a polycrystalline material, which typically has a size much larger than that of a crystalline grain. A polycrystalline material is an aggregate formed by a large number of crystalline grains (disjoint but closely packed among themselves), which are randomly oriented relative to one another. It follows that the optical anisotropy properties of one crystalline grain in the aggregate tend to be compensated for by those of the surrounding ones. Then, the average (macroscopic) optical properties of the polycrystalline material may appear to be approximately isotropic.[1]

A liquid crystal has no positional order, but it displays an orientational one. That medium is formed by molecules, for each of which the structure and properties are not the same for different directions in principle, as commented above. The positions of the different molecules in the liquid are fully random. However, the orientations of those (anisotropic) molecules may turn out to be not completely random. It follows that, by virtue of that orientational order, the medium is anisotropic and, in particular, the liquid crystal turns out to be optically anisotropic.[3]

2.4 OPTICAL ANISOTROPY(II): FORM BIREFRINGENCE

A different and quite interesting case of optical anisotropy is form birefringence,[1] which can be described as follows. The electrical properties of atoms and molecules are typically anisotropic. Let s_{is} be some bound system formed by a sufficiently large number of those (individually anisotropic) atoms and molecules, which has a size naturally large compared to typical molecular dimensions and, on the other hand, small compared to the wavelength of light. We also suppose that s_{is} turns out to be optically isotropic (so that the anisotropies of the molecules constituting s_{is} cancel out with one another, on the average).

Let S_{anis} be another system of larger size, constituted by an ordered arrangement of a certain number of similar bound subsystems, each of the them identical to s_{is}. To fix the ideas, we shall also suppose that the separations among neighboring subsystems of type s_{is} in the assembly S_{anis} are smaller than typical wavelengths of light. Then, it follows that the ordered arrangement S_{anis} appears to display optical anisotropy (in some effective sense, as explained below).

Two explicit idealized models, displaying that anisotropy phenomenon, have been analyzed in certain detail. Several important, and by now classical, results have been obtained by Lord Rayleigh and O. Wiener, and we refer to Born and Wolf[1] for an account of them. Another clear presentation has been made by Harosi.[21] In one model (model p), s_{is} is chosen to be a thin plate, while S_{anis} is a regular assembly of parallel plates, all identical to s_{is}. A key role is played by the axis perpendicular to the planes of the plates (optic axis). In the second model (model r), s_{is} is a thin cylindrical dielectric rod and S_{anis} is an assembly of rods with parallel axes, all similar to s_{is}. Then, an axis parallel to those of the rods is important (optic axis). For either of those two models, let us suppose that a plane electromagnetic wave is incident on S_{anis}. For both models, illumination (the wave vector of the incoming light) is perpendicular to the corresponding optic axis. The wavelength (in the typical optical range) is supposed to be larger than: i) either the thickness of the plates (model p) or the transverse diameter of the rods (model r), and ii) typical separations between two neighboring plates or rods, as commented above.

For both models, let the electric field of the electromagnetic wave be perpendicular to the corresponding optic axis: ordinary (o) wave case. Then, let ϵ_o be the effective dielectric permittivity of the assembly S_{anis} (after having performed suitable averages), for both models. Next, and also for both models, we suppose that the electric field of the electromagnetic wave is parallel to the corresponding optic axis: extraordinary (e) wave case. For both models, let ϵ_e be the (effective) dielectric permittivity of the assembly S_{anis}. We remark, in order to facilitate the comparison with Born and Wolf,[1] that the dielectric permittivities considered in this section are not the relative ones, that is, they equal ϵ_0 multiplied by the corresponding relative dielectric permittivities. It follows that:[1] i) $\epsilon_e - \epsilon_o \neq 0$, ii) then, S_{anis} behaves as a uniaxial optically anisotropic system. Such an anisotropy (on a scale much larger than the molecular one) is named form birefringence. Quantitatively, the latter is characterized by the coefficient $\epsilon_e - \epsilon_o$ or by the equivalent expression that results if dielectric permittivities are replaced by refractive indices (so that those dielectric permittivitties times μ_0 equal the corresponding squared refractive indices).

For model p, let us consider a medium consisting of plates of refractive index n_1 and fractional volume f_1 embedded in a surrounding substance of index n_2 and fractional volume f_2. f_1 and $f_2(= 1 - f_1)$ are the fractions of the total volume occupied by the plates and by the surrounding medium, respectively. Then:

$$n_e^2 - n_o^2 = -\frac{f_1 f_2 (n_1^2 - n_2^2)^2}{f_1 n_2^2 + f_2 n_1^2} \tag{2.5}$$

For model r, let us consider a medium consisting of small, parallel, well-separated rods of refractive index n_1 and fractional volume f_1 embedded in a surrounding substance of index n_2 and fractional volume f_2. f_1 and f_2 are, as in the above case of model p, the fractions of the total volume occupied by the rods and by the surrounding medium, respectively. In the actual case (model r), it is assumed that $f_1 \ll 1$. Then, the form birefringence coefficient is approximately:

$$n_e^2 - n_o^2 = \frac{f_1 f_2 (n_1^2 - n_2^2)^2}{(1 + f_1) n_2^2 + f_2 n_1^2} \tag{2.6}$$

In this formula, there is no restriction on the refractive index difference between the rods and the surrounding substance.

We stress that in both Eqs. (2.5) and (2.6), n_e is the (extraordinary) refractive index for light linearly polarized parallel to the optic axis. n_o is the (ordinary) refractive index for light linearly polarized perpendicular to the optic axis. See Born and Wolf[1] and references therein. Notice that the right-hand side of Eq. (2.5) is negative ("negative uniaxial crystal") while that of (2.6) is positive ("positive uniaxial crystal").

The phenomenon of form birefringence has some important applications in biological microscopy. For instance, the experimental measurement of that optical anisotropy (that is, of those effective dielectric permittivities) may yield information regarding the form of s_{is}, the fraction of volume occupied by all s_{is} (over that of the surrounding medium in which they are located).

The form birefringence phenomenon has continued to attract further interesting researches. We shall limit ourselves to quote three of them, to which we refer for a wider perspective and, in turn, for further references. The form birefringence of lamellar systems containing three or more components has been studied by Thornburg.[22] The form birefringence of an array of parallel cylinders of arbitrary sizes and separations, under the assumption of small variation among the refractive indices of its components, has been analyzed further by Hemenger:[23] a new expression for the form birefringence coefficient of that assembly has been obtained. The latter expression depends on the correlation function of the fluctuations in refractive index through the medium (those fluctuations being small, by assumption). Such a formula,[23] which applies for cylinders with dimensions comparable to or greater than a typical wavelength of light, generalizes Eq. (2.6). Further interesting investigations of form birefringence for thin fibers and membranes have been carried out by Zhou and Knighton.[24]

2.5 OPTICAL ANISOTROPY(III): PHOTO-ELASTIC EFFECT

Another important class of optically anisotropic dielectric media results when originally (unstressed) isotropic materials are subject to mechanical stresses. The latter could be due to externally applied forces. Internal mechanical deformations are produced in those materials which, in turn, give rise to optical anisotropies. This is frequently referred to as the photo-elastic effect.[3] It is also known as stress birefringence[1] and dynamo-optical effect.[2]

Brewster provided evidence of the photo-elastic effect through a fundamental experiment.[25] See the quite interesting discussion in Bruhat.[26] The photo-elastic effect is documented in some already classical monographs.[27,28]

We shall discuss some general features of stress birefringence.[2] Let us consider a solid medium at rest and at equilibrium, which appears to behave as isotropic (both from the mechanical and optical standpoints), as a zeroth-order approximation. Then, the dielectric permittivity tensor $\tilde{\epsilon}$ of the material relative to that of another (optically isotropic) reference material is: $\epsilon_{ij} = \epsilon_e \delta_{ij}$, $i, j = 1, 2, 3$. ϵ_e is the relative (dimensionless) dielectric permittivity of the solid medium and δ_{ij} denotes the Kronecker delta symbol ($\delta_{ii} = 1, \delta_{ij} = 0$ if $i \neq j$). In the latter description, one neglects possible small local deformations of the material due to internal stresses. In the application of specific interest in this article, the reference material will have dielectric permittivity ϵ_0 and be chosen as the surrounding medium in which the above solid one (in the form of one or several waveguides) will turn out to be located.

A more accurate description of that solid medium requires us to take into account small elastic deformations in it (arising from small elastic stresses, in the domain of reliability of Hooke's law.[29]) Those small deformations are potentially important for the optical behavior of the solid medium since, in principle, they give rise to some (small) optical anisotropy. This is the photo-elastic effect.

In order to outline a quantitative description of such an effect, a few notions of elasticity theory are required,[29] to which we now turn. The deformed solid medium is also supposed to be at rest and at equilibrium, for the small elastic deformations to be considered here. Let us consider, in the absence of deformations in the solid medium, a generic small volume element of it ($dx_1 dx_2 dx_3$), located at the generic position $\bar{x} = (x_1, x_2, x_3)$. When the solid medium is subject to small deformations, that small volume element becomes a new small one ($dx_1' dx_2' dx_3'$), located at the new position $\bar{x}' = (x_1', x_2', x_3') = (x_1 + u_1, x_2 + u_2, x_3 + u_3)$. $u_i = u_i(x_1, x_2, x_3)$ is the displacement, which will always be assumed to be small. Let $u_{ik} = u_{ik}(x_1, x_2, x_3)$, $i, k = 1, 2, 3$, be the (small) components of the deformation tensor in the deformed solid medium. They are given in terms of the displacements u_i, since the latter are small, as follows: $u_{ik} \simeq 2^{-1}(\partial u_i/\partial x_k + \partial u_k/\partial x_i)$. To grasp the physical interest of u_{ik}, we shall limit ourselves to recall that the size of the new (deformed) small volume element is given, in terms of the one before deformation, as follows: $dx_1' dx_2' dx_3' \simeq dx_1 dx_2 dx_3 (1 + \sum_{i=1}^{3} u_{ii})$. Notice that $u_{ik} = u_{ki}$ and that all u_{ik} are dimensionless.

The small deformations are caused by small internal elastic stresses. Specifically, small internal elastic forces act upon any given volume element of the deformed solid medium, due to the rest of the material. The physical origin of all those internal elastic forces could be some force applied externally to the solid material under consideration. A reliable physical idea is that the net result of all those internal forces on that volume element acts across its boundary (and also that the external force applied to the solid material acts across its external surface).[29] This idea implies that the net elastic force per unit volume (F_1, F_2, F_3), on a small domain (having volume $dx_1 dx_2 dx_3$) of the deformed solid medium is given by $F_i = \sum_{k=1}^{3} \partial \sigma_{ik}/\partial x_k$. $\sigma_{ik} = \sigma_{ik}(x_1, x_2, x_3)$ is the stress tensor, and it has dimension *force/(surface area)*. It is symmetric ($\sigma_{ik} = \sigma_{ki}$), under suitable conditions,[29] which are supposed to hold here. A basic approximation that holds for small deformations is a suitable linear relationship between the components of the stress tensor and those of the deformation one and conversely (Hooke's law). Hooke's law, expressed as that linear relationship and its inverse, reads:[29]

$$\sigma_{ik} \simeq \left(\lambda_{La} + \frac{2\mu_{La}}{3}\right)\delta_{ik} + 2\mu_{La}\left[-\frac{1}{3}\delta_{ik}\sum_{l=1}^{3} u_{ll} + u_{ik}\right] \tag{2.7}$$

$$u_{ik} \simeq \frac{1}{9(\lambda_{La} + (2/3)\mu_{La})}\delta_{ik}\sum_{l=1}^{3}\sigma_{ll} + \frac{1}{2\mu_{La}}\left[-\frac{1}{3}\delta_{ik}\sum_{l=1}^{3}\sigma_{ll} + \sigma_{ik}\right] \tag{2.8}$$

λ_{La} and μ_{La} (both positive and with dimension *force*/(*surface area*)) are constants, characteristic of the solid medium. They are known as the Lame coefficients.

We shall now come back to our main subject, namely optics. When the effects of small elastic deformations of the solid medium are taken into account as discussed above, one accepts that the relative dielectric permittivity tensor of the latter medium is:[2]

$$\epsilon_{ij} \simeq \epsilon_e \delta_{ij} + a'_1 u_{ij} + a'_2 \left(\sum_{l=1}^{3} u_{ll} \right) \delta_{ij} \tag{2.9}$$

a'_1 and a'_2 are (dimensionless) photo-elastic constants, characteristic of the deformed medium, and u_{ij} is its deformation tensor. It is convenient to recast the above ϵ_{ik} in terms of the stress tensor σ_{ik}, by using Hooke's law (Eq. (2.8)). One finds easily:

$$\epsilon_{ik} \simeq \epsilon_e \delta_{ik} + a_1 \sigma_{ik} + a_2 \left(\sum_{l=1}^{3} \sigma_{ll} \right) \delta_{ik} \tag{2.10}$$

where a_1 and a_2 are elastic-optical constants (with dimension (*surface area*)/(*force*)). They are given, in terms of the above a'_1 and a'_2, by:

$$a_1 = \frac{a'_1}{2\mu_L}, a_2 = -\frac{\lambda_L a'_1}{2\mu_L(3\lambda_L + 2\mu_L)} + \frac{a'_2}{3\lambda_L + 2\mu_L} \tag{2.11}$$

As an example, we quote the following values of a_1 and a for silica: $a_1 = 0.38 \times 10^{-12}$ $m^2/Newton$ and $a_2 = 2.68 \times 10^{-12}$ $m^2/Newton$. The photo-elastic effect has certain interesting consequences regarding optical wave propagation in waveguides formed by such materials.[20,30,31]

2.6 HIGHLY BIREFRINGENT WAVEGUIDES

We shall review a few interesting aspects of propagation modes in an ideal optically isotropic homogeneous fiber with circular cross-section of radius R and refractive index n_{co}. That waveguide is placed in another homogeneous optically isotropic medium (cladding) with refractive index $n_{cl} (< n_{co})$. Let light, with wavelength λ, propagate confined along the fiber. One introduces the useful dimensionless parameter

$$V = \frac{2\pi R}{\lambda} \left(n_{co}^2 - n_{cl}^2 \right)^{1/2} \tag{2.12}$$

The fundamental (or lowest order) mode is degenerate, that is, there are two lowest order polarization modes (denoted as HE_{11}^x and HE_{11}^y), orthogonal to each other and with the same spatial intensity distribution: they both correspond to $0 < V < 2.40$. The next four modes of first order correspond to $2.40 \leq V < 3.83$: they are denoted as TE_{01}, TM_{01}, HE_{21}^{even} and HE_{21}^{odd}. Suitable linear combinations of these are also currently employed, in order to describe the set of four first order modes, just above the two ones of zeroth order (namely, the fundamental ones). The set of all propagation modes of second order correspond to $3.83 \leq V < 5.13$. For single-mode or monomode optical fibers, only the (degenerate) fundamental mode propagates.

Perturbations (induced by pressure, strain, bend, twist, temperature, . . .) in a real or non-ideal waveguide eventually upset the properties of the propagation modes in it. Let us consider a real (non-ideal) homogeneous optically isotropic homogeneous fiber with circular cross-section, and let us suppose that it corresponds to a monomode waveguide (say, $V < 2.40$). Let light penetrate into it and start to propagate confined along it, in a definite polarization state corresponding to one of the degenerate fundamental modes. Estimates indicate that, due to those perturbations in the real fiber and after propagation through a length about 1 m, the polarization of the initially launched fundamental mode will be modified in an unpredictable way. The control of that polarization state launched into the monomode waveguide turns out to be essential for efficient performance. This has led to an added recognition of the importance of polarization and of its preservation in those single-mode fibers. Single-mode optical waveguides, in which the polarization state of its propagating modes is preserved to a high degree, have acquired an increasing technological importance in the last two decades, in particular through their applications for optical communications, as high-performance polarimetric optical fibers and sensors.

Research on confined propagation in optically anisotropic dielectric waveguides has arisen from attempts to preserve (linear) polarization of the propagation modes in single-mode optical fibers. That preservation has been attempted in two ways. One has been the minimization of the stress-induced birefringence.[32] The other has been to maximize birefringence, which breaks the degeneracy of the fundamental modes. The latter can be accomplished: i) by introducing asymmetric profiles for the refractive index distribution (for instance, through non-circular shapes of the transverse cross-sections of the waveguides),[33,34] and ii) through anisotropic internal stresses.[34,35] Just as an example, we note that a proposal has been reported[18] about confined propagation modes in twisted fibers. The twist gives rise to shearing stresses which, in turn, introduce optical anisotropy: the dielectric permittivity becomes a tensor (photo-elastic effect). For a sufficiently large twist, the propagation modes in the anisotropic fiber retain a high degree of polarization, as analyzed theoretically and demonstrated experimentally. There is a very active and well documented research[36] on birefringent dielectric waveguides aimed at improving optical devices.

Over the last two decades, there have been an increasing number of proposals for producing sensor optical waveguides and characterizing significant thermal and mechanical parameters like temperature tolerance and elasticity and optical properties, such as refractive index distribution.[37]

The basic idea of stress sensing by means of optical fibers is the following. Let us consider a dielectric fiber that had been optically isotropic first and, at a later stage became optically anisotropic. The latter behavior has been due to some externally applied force, giving rise to the photo-elastic effect in that fiber. Let light beams propagate confined along the waveguide, first when the latter was optically isotropic and, later, when it became optically anisotropic. Upon analyzing comparatively the features of both confined beams, physically relevant information can be obtained about the state of stress of the anisotropic waveguide, and, eventually, about the external force that has given rise to it. Alternatively, one could scatter light by the fiber, first when it was optically isotropic and, later, when it had been perturbed, by developing the optical anisotropy. Suitable differences between the light scattering distributions in both cases can now yield information about the additional internal stress of the perturbed waveguide and its cause (the external force on it).

In many applications in civil engineering (mining, construction projects, concrete structures), it is important to evaluate the response of a structure for safety purposes and damage assessment. Sensing pressure in those environments can be acomplished very efficiently by using technology based upon optical fiber sensors, specifically those employing highly birefringent waveguides (polarimetric sensors). Similar statements appear to apply to evaluating machinery in engineering mechanics and aerospace industries (strains in advanced aircraft and space vehicles). One very interesting possibility consists of embedding sensors based upon highly birefringent fibers into the structures of composite materials.

Different kinds of optical fiber sensors based upon the confined propagation of light for stress sensing have been investigated, for example, interferometric and grating-based systems.[36]

In previous work on light scattering applied to stress sensing, experimental determination of backward-scattering data yielded information on the refractive index distribution. Therefore, changes in the latter due to stresses and strains could be detected by analyzing the distribution of the scattered radiation at 180°.[38]

2.7 BIOLOGICAL WAVEGUIDES IN THE EYE

The interaction of light with biological tissues as dielectric matter in the eye has enormous relevance, at least: i) in order to understand the behavior of some very important biological phenomena, and ii) for its application as an optical method to investigate certain, also very important, elements in the eye, under both normal and pathological functioning conditions. We shall limit ourselves to discussing a few general aspects.

The retina is a soft biological tissue with thickness smaller than about 0.5 mm and transparent to light.[16] Its outermost part is the pigment epithelium (in which the optical image is formed), and its innermost part (the inner limiting membrane) is connected to another crucial part of the eye system, namely the optic nerve. The connection between those inner parts of the retina and the optic nerve is named the optic disk.

Leaving aside other elements in the retina, we shall focus on the retinal photoreceptors (that start below the pigment epithelium and are roughly perpendicular to it) and on the retinal nerve fiber layer (which is just above the inner limiting membrane). Input light that penetrates into the eye through the cornea and traverses the pigment epithelium enters into the retinal photoreceptors and propagates confined along them. At some later stage, and through some involved processes (not to be discussed in this chapter), light is absorbed by certain organic molecules (rhodopsin) and the resulting output biological signal is transmitted to the optic nerve. There are two kinds of photoreceptors: the rods (operating maximally at low light intensities, say, at night) and the cones (operating maximally at high light intensities and in color vision). Some features of the retinal nerve fiber layer and some further ones of photoreceptors will be commented on later in this section.

The retinal photoreceptors and the retinal nerve fiber layer are very complex structures. Following previous researchers[16] and as a zeroth-order approximation, one models the retinal photoreceptors as arrays of approximately parallel cylindrical dielectric waveguides (each having a length larger than its transverse diameter). Qualitatively similar models (but unrelated to those for photoreceptors) will be assumed for the elements of which the retinal nerve fiber layer is composed.[24]

In order to motivate our further discussions in this section, we shall simply notice that the macula (a central part of the retina) has significant involvement in ocular pathology and can display considerable birefringence. The measurement of birefringence in the macula may indicate the existence of a pathology.[23]

In the following subsections of this section, we shall offer a qualitative partial overview of various arrays of (more or less) approximately parallel cylindrical dielectric waveguides located inside the eye (in the cornea and in the retina). The propagation of light inside the eye gives rise to certain important phenomena in those arrays, which will also be discussed in those subsections. The average refractive index of the retina (regarded as a surrounding biological medium in which the various retinal waveguides are embedded) is about 1.34 (very close to that for water).[39] Other authors take 1.36 an as average value for the refractive index of the retina.[24] See also Subsection 2.7.1. The various retinal waveguides are regarded as optically isotropic, at least as a zeroth-order approximation in normal functioning conditions. In other situations (namely, beyond the zeroth-order approximation in normal functioning conditions or in pathological functioning ones), optical anisotropy may be considered or does arise. Form birefringence and scattering occur. Multiple scattering effects can be approximately neglected in some situations, but not in others.

We note that the presence of some birefringence in retinal photoreceptors and in the nerve fiber layer of the human retina appears to be known from various experimental data and procedures. That birefringence is associated, at least to a certain degree with dichroism[1,21] in the material structure. We employ the term *dichroism* to refer to different amounts of absorption by the material for various light beams propagating through it and polarized in different directions. For our purposes (and, at least, in a qualitative or general sense), we may understand such dichroism by recalling that the components ϵ_{ij} of the relative dielectric permittivity tensor were allowed to be complex. Dichroism is anisotropy in absorption. Let a composite body, formed by light- absorbing particles, be similar to those described in Section 2.4 (the wavelength of light being also adequately larger than typical dimensions). Then, the composite body may exhibit anisotropic absorption of light (form dichroism).[21]

2.7.1 Scattering by Cylindrical Waveguides in Cornea

The normal cornea is nearly transparent to light, except for some (weak) scattering phenomena which occur in it. The corneal stroma (the tissue forming its ground substance) is formed by stacked sheets (named lamellae). Each sheet contains long thin parallel collagen fibers (fibrils), embedded in a ground substance (composed of glycosaminoglycans in a salt solution). The ground substance can be regarded to be optically homogeneous. The fibril axes are parallel to the surfaces of the cornea. Fibrils in normal or swollen corneas seem to have essentially the same diameter (about a few tens of nanometers, nm), while those in scarred corneas have a rather wide range of diameters. The distribution of fibrils in a normal cornea is different from those for swollen corneas. Light propagating through the cornea is scattered by the individual fibrils. Scattering phenomena in normal corneas will be different, eventually, from those taking place in swollen or scarred corneas. The scattering of light by the fibrils in a normal cornea, in the so-called Debye-Born-Rayleigh-Gans approximation (to be discussed in Sections 2.8 and 2.10) for each individual fibril, has been studied.[40] The fact that the fibrils in a normal cornea do not behave as independent scatterers gives rise to important cancellations in the differential cross-section. The latter, in turn, account for the near transparency of a normal cornea. Smaller cancellations would take place for scatterings in swollen or scarred corneas, which would imply less transparency for them.[40] Multiple scattering in the cornea has been investigated,[41] and birefringence in the cornea has been studied.[42] See also next subsection.

2.7.2 Retinal Nerve Fiber Layer: Form Birefringence and Scattering

The retinal nerve fiber layer (that part of the retina that is connected to the optic nerve) is a complex structure which, regarding light propagation, is nearly transparent and behaves as weakly reflecting. Consequently, the retinal nerve fiber layer scatters some light (to a certain limited extent). It seems that such a scattering is due to structures (cellular organelles), approximately cylindrical and parallel to one another that are distributed throughout the thickness of the retinal nerve fiber layer. Cellular organelles at the retinal nerve fiber layer (RNFL) provide another important example of approximately parallel cylindrical biological waveguides as microtubules.[24]

As revealed by electron microscopy, the RNFL contains bundles of nerve cells (nerve-cell axons) that run just under and across the surface of the retina. A nerve fiber bundle contains four different kinds of approximately cylindrical structures: a) axonal cell membranes around nerve axons (axonal membranes), b) microtubules, c) neurofilaments, and d) mitochondria. Those structures lie in a rather complex cellular environment (some aqueous solution of proteins and other cellular constituents). Within the scope of this chapter, it is interesting to describe briefly those structures and their sizes.[24]

Axonal membranes are thin phospholipid bilayers (with transverse sizes about 6 to 10 nm) that form cylindrical shells enclosing the axonal cytoplasm. Microtubules are long (10 to 25 microns) tubular cylinders of the protein tubulin; they have inner and outer diameters about 15 and 25 nm, respectively. Neurofilaments are stable proteins, having a diameter about 10 nm. Mitochondria are ellipsoidal organelles that contain membranes of lipid and protein: their length and thickness are about 1 to 2 microns and about 100 to 200 nm, respectively. It follows that the transverse dimensions of axonal membranes, microtubules and neurofilaments are appreciably smaller than typical wavelengths of light (thin fibers) while those of mitochondria are not. The typical separations between two neighboring cylindrical structures of those kinds appear to be smaller than the wavelength of light.

The refractive indices of the various organelles in the RNFL range from about 1.36 up to about 1.64.[24]

The resulting arrays of approximately parallel cylinders appear to display some form birefringence: compare with Section 2.4 (model r). Then, cellular organelles at the retinal nerve fiber layer (RNFL) provide an example of optical anisotropy.[24]

To appreciate the potential interest of researchers about light scattering by the latter cylindrical structures, we shall limit ourselves to point out the following. The retinal nerve fiber layer is damaged in glaucoma and other diseases affecting the optic nerve. Detectable modifications of the retinal nerve fiber layer (say, its thinning) may occur before losses of vision become manifest and measurable. Then, optical methods that enable us to assess the state (thickness) of the retinal nerve fiber layer may provide aids for diagnosis. The optical methods involved include the analysis of the reflected light (arising from its scattering by the retinal nerve fiber layer into the backward direction).[24]

Further and interesting discussions of form birefringence for the RNFL arose,[24] by means of a relatively recent formula for an assembly of parallel cylinders. Some detailed analysis of the scattering of light by the organelles in the RNFL, each of them treated as an optically isotropic waveguide, have also been carried out in the same investigation.[24]

Various experiments implying birefringence in the RNFL have been reported in recent decades.[43,44] Other experiments,[45] using a laser ellipsometry technique demonstrated that the RNFL of the human retina exhibits substantial uniaxial birefringence. Additional studies have demonstrated that the RNFL possesses dichroism (interpreted possibly, as form dichroism, due to microtubules and neurofilaments).[46] Those studies[45,46] also deal with birefringence and dichroism in the cornea.

2.7.3 Retinal Photoreceptors

Retinal photoreceptors in the eye can be regarded at least as a zeroth order of approximation, as arrays of optically isotropic cylindrical dielectric cylinders with circular cross-sections of radius R.[16,17] The transverse diameters of the various photoreceptors can be taken to vary between about 0.6 μ m and about 2 μ m. The average separations between two neighboring photoreceptors can be regarded be to about 0.5 μ m (or, at most, a bit larger, up to about 2 μ m).

Let n_1 and n_2 be the refractive indices of the photoreceptor and of the surrounding medium, respectively.

The refractive indices n_1 of the various photoreceptors have been estimated to range from about 1.36 up to about 1.41.[16] One may also estimate the value for n_1 as 1.35, since the fibers of the RNFL (see Subsection 2.7.2) are not coated with white matter or myelin. The considered value corresponds more to "grey matter" or axonal material.

The refractive index n_2 of the surrounding medium can be estimated as follows. As established earlier by Sidman,[39] the interstitial organic material surrounding a biological waveguide has a refractive index very close to that for water (H_2O): $n_2 = n_{H_2O} + \alpha C$. α is a numerical coefficient and C is the percentage of concentration of solids (proteins, lipoproteins or lipids). We point out that α is rather stable for bio-materials, and $|\alpha C| << 1$. Since: $n_{H_2O} = 1.3334$, we assume $n_2 \simeq 1.34$ (for a wavelength of light in free space corresponding to an average over the visible spectrum, namely, for $\lambda = 0.5\ \mu$m). Notice that 1.34 is also used as a value for the refractive index of the cytoplasm (see, for example, Sidman[39] and references therein). Thus, the refractive indices of the various photoreceptors minus that of the surrounding medium (say, the average refractive index of the retina) in which the former are embedded may be about 0.01.

As was established by Enoch,[16] optical photoreceptors are guiding light under conditions of total internal reflection and behave as waveguides under ordinary conditions (normal functioning). In a geometrical optics description, light that has penetrated into one photoreceptor is guided along it subject to successive total internal reflections. In the electromagnetic wave description, light propagates confined along the photoreceptor in the form of propagation modes. For photoreceptors with circular cross-section of radius R, each set of modes is characterized by the values of the so-called V parameter given in Eq. (2.12), where: $n_1(= n_{co})$ and $n_2(= n_{cl})$ are the refractive indices of the photoreceptor (core) and of the surrounding media (cladding), discussed above, and $2R$ is the diameter of the photoreceptor. In more technical terms, the V parameter determines the specific cut-off frequency for the corresponding set of modes.[10] We consider $2R \simeq 2.0\ \mu$m.

It is accepted that human optical photoreceptors (regarded, in a zeroth order approximation, as homogeneous optically isotropic dielectric fibers of circular cross-section) support about six propagation modes. The latter include the set of two fundamental modes (zeroth order) and other higher order modes (first and second order ones).[16] Recall the short summary about propagation modes in Section 2.6. Modes of order two or higher transport a much smaller percentage of energy than the fundamental ones.[17] For a waveguide supporting low-order modal patterns, as is the case with human receptors, one may take $0 < V < 10.9$, where the upper limit has been taken as rather high, so as to include a set of low order modes.

The absorption of light by the organic material in photoreceptors during the confined propagation appears to be small and it constitutes an interesting phenomenon.

Birefringence and dichroism in retinal photoreceptors have been established and analyzed in detail.[21]

Mitochondria may introduce (small) anisotropies in photoreceptors.[47]

The birefringence of biological waveguides and, in particular, of retinal optical photoreceptors has been studied and measured by several authors during recent decades by using various techniques in mammalians and also for the human eye.[39,48] The birefringence in biological waveguides is due to the particular assembly of anisotropic organic molecules constituting the material of each one of the segments forming the whole waveguide structure and to the photochemical properties of the components. Recall that for the RNFL, Dreher et al.[45] measured the degree of preserved polarization and amount of dichroism as functions of angular position of measurement locations in eight postmortem human eyes. The authors obtained two maxima that correlate with the areas of the thickest RNFL.

To summarize, one can make a quantitative assessment of the amount of birefringence by means of the so-called net birefringence (Δn), which is a suitable sum of differences of refractive indices (each difference being due to a specific physical effect). A non-vanishing value for the net birefringence ($\Delta n \neq 0$) is a manifestation of overall optical anisotropy. In principle, the net birefringence is the sum of the intrinsic, form and chromatic birefringences: $\Delta n = \Delta n_I + \Delta n_F + \Delta n_C$. We anticipate that the contribution of the chromatic birefringence (Δn_C) will be neglected.

Liebman[48] succeeded in measuring the intrinsic (Δn_I), form (Δn_F) and net birefringence (Δn) in unbleached and bleached rod outer segments (ROS) in *R. Pipiens*. He assumed that the ROS behaves as a uniaxial crystal. By measuring the percentage of retardation of light, he found for the net birefringence: $\Delta n \simeq +0.0015$ (for a wavelength of light in free space $\lambda = 0.5\ \mu$m). Since birefringence depends on wavelength, we can estimate $\Delta n \simeq +0.0010$ for $\lambda = 0.68\ \mu$m , by following the mentioned results. The measured value of the net birefringence is affected by contributions with negative signs. It turns out that Δn_F takes on negative values.

For the purposes of characterizing the birefringence, one needs particular experimental values of $\Delta n_F = n_e - n_o = c/v_e - c/v_o$, where v_e and v_o are the velocities associated with the extraordinary and ordinary rays, respectively, in relation with the direction of the optic axis. We notice that the measured experimental values used to be very much influenced by the experimental procedure and by photochemical reactions induced in the structure of the organic components of the waveguide at the time of carrying through the measurements.

At this point, let us recall the form birefringence coefficient given in Eq. (2.5), which turns out to be negative. In the case of interest for us here, this behavior could correspond, for example, to the real lamellar structure originated by the disposition of fibers (n_1) and the interstitial matrix (n_2) in the array of the RNFL of the retina (polarization properties) as theoretically considered in the present study ($n_1 > n_2$). In so doing, we are identifying (or approximating) these n_1 and n_2, respectively, with the values for the refractive indices of the photoreceptor (n_1) and of the surounding medium (n_2), discussed previously in this subsection. Upon proceeding with the form birefringence coefficient given in Eq. (2.5), let $f_1 = f_2 = 1/2$ (namely, the case of two components with equal fractional volumes) and we consider small birefringence, so that $n_e + n_o \simeq n_1 + n_2$. Then, the form birefringence coefficient given in Eq. (2.5) (actually, a simplification of Wiener's formula[1]) yields the following approximate formula for the form birefringence:

$$\Delta n_F = n_e - n_o \simeq = -\frac{(n_1 - n_2)^2 (n_1 + n_2)}{2\left(n_1^2 + n_2^2\right)} \tag{2.13}$$

This behavior is characterizing a particular form birefringence.[45] See Figure 2.1. We observe that Δn_F has negative small values (negative uniaxial crystal).

Thus, from a theoretical point of view, this degree of birefringence of photoreceptors (for one single receptor) is related to their waveguiding properties.

The degree of birefringence is also a function of the V parameter of the waveguide: $n_1 = n_1(V)$. In order to understand this dependence, we have analyzed the behavior of $\Delta n_F = \Delta n_F(V)$, for two values of the wavelength: $\lambda = 0.6328\ \mu$m and $\lambda = 0.5\ \mu$m. For a fiber behaving as a single mode waveguide (or for $0 < V \leq 4$), the difference of the values of Δn_F for those two close values of λ appears to be very small (almost zero). On the other hand, as we approach the behavior of the fiber as multimode supporting two sets of modes or as V increases (say, for $6 < V \leq 10$), the

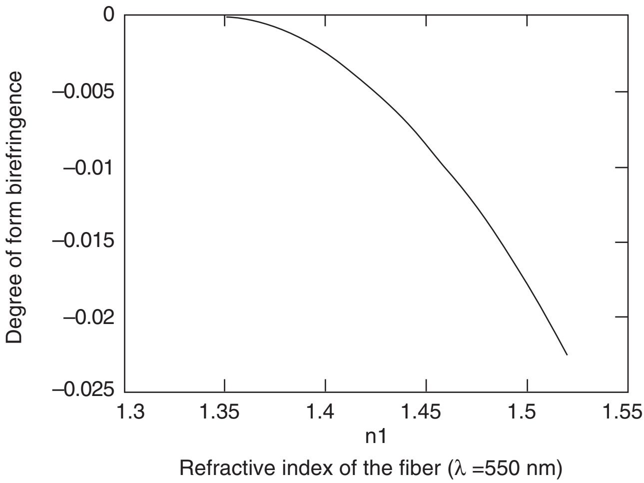

FIGURE 2.1 Behavior of Δn_F as a function of the refractive index n_1, for a wavelength $\lambda = 0.55$ μm of light.

difference between the two values of Δn_F for those two wavelengths dramatically increases as V does.

Assuming that $n_2 \simeq 1.34$ and $\Delta n_F = -0.009$ (as theoretically calculated by Harosi,[21]) we can observe that this value is obtained for $V = 8.4$ (< 10.9) for $\lambda = 0.5$ μm and $V = 6.6$ ($\lambda = 0.6328$ μm). From this result, we can interpret that the value $\Delta n_F = -0.009$ is acceptable, and the fiber is far from being considered as a single mode one. Nevertheless, it is not warranted, *a priori*, that all allowed high-order propagation modes will be effectively excited. We can still keep the single mode approximation for the sake of simplicity of the present model.

Notice that in order to obtain positive values for Δn, we still need to include the additional contribution corresponding to the intrinsic birefringence properties of the concentration of solids along the axial direction of the fiber (in particular, lipid molecules), namely, Δn_I. Upon neglecting the chromatic birefringence, we have $\Delta n \simeq \Delta n_F + \Delta n_I$. Specifically, in order to obtain the positive experimental values reported in the literature ($\Delta n \simeq 0.0015$), and since $\Delta n_F = -0.009$, one has $\Delta n_I = 0.0105$, corresponding to a higher birefringence value. The latter, in turn, may be originated by a permanent organization of lipid molecules.

Let us regard each photoreceptor as a uniaxial birefringent medium in the form of a cylindrical waveguide and assume the x_3 axis lies along the axis of the waveguide. The values of the non-diagonal elements of the relative dielectric permittivity tensor are associated with optical activity (related, in turn, to the presence of non-symmetric molecules). At this point, we can mention that rhodopsin contains non-symmetric molecules like α-helical structures. A measurement of the optical activity can be performed by determining circular birefringence, but the importance of the induced phenomenon would be very weak.[21] Then, one may estimate approximately that, in the actual case, the corresponding relative dielectric permittivity tensor has $\epsilon_{12} \simeq 0$.

There are some important effects regarding the capture of light by retinal photoreceptors and visual response. One of them is the Stiles-Crawford effect of first kind (*SCE-I*) that evidences the behavior of retinal photoreceptors as antennas and optical dielectric waveguides.[16,17] In the *SCE-I*, the profile of the experimental intensity distribution of the luminous energy scattered by the retinal photoreceptors exhibits a maximum in the direction of the center of the eye pupil. For the particular case of the *SCE-I*, and due to the limited range of the measured angles (limited eye pupil), the experimental results turn out to correspond to a selective angular range that is close to the forward scattering direction. The numerical representation of the angular distribution of the luminous energy evidences a maximum for the forward scattering direction. This result indicates the orientational properties of groups of retinal photoreceptors.

Recall that the receptor orientation is the result of several forces: a) phototropic (orienting the photoreceptors toward the center of the pupil), b) a force perpendicular to the retinal epithelium (for alignment of the photoreceptors toward the center of the retinal sphere), c) retinal tractions, and d) receptor packing. Results obtained earlier for the *SCE-I* in observers having ectasia (Fuch's coloboma) show receptor alignment abnormality or disturbance.[49]

Further experimental results in relation to the *SCE-I*, with dramatic changes of the data have revealed systematic strains causing orderly alterations in photoreceptor orientations in observers with high myopia.[50] One possible qualitative explanation of the latter experimental results could be that, under such anomalous conditions (high myopia), some optical anisotropy (implied by the photo-elastic effect) could have arisen in those biological cylindrical waveguides, namely in the retinal photoreceptors and in the retinal nerve fiber layer.

2.8 CLASSICAL ELECTROMAGNETIC SCATTERING BY ANISOTROPIC OBJECTS IN ISOTROPIC MEDIUM

Let us consider in three-dimensional space an infinite isotropic and homogeneous dielectric reference medium, that has real constant dielectric permittivity ϵ_0, zero electrical conductivity, magnetic permeability equal to that of vacuum (μ_0, real) and, hence, constant refractive index n_0. We also consider N separate (non-overlapping) optically anisotropic dielectric objects (with arbitrary shapes and relative orientations with respect to one another) located at fixed positions in the reference medium. Each object has zero electrical conductivity, magnetic permeability equal to μ_0 and a (symmetric) dielectric permittivity tensor $\epsilon_0 \cdot \tilde{\epsilon}$, where $\tilde{\epsilon}$ is the dielectric permittivity tensor of the object relative to that of the surrounding reference medium. ϵ_{ij} is, in general, complex.

We shall suppose that each ϵ_{ij} and its first spatial derivatives are continuous everywhere, that is, also across the interface separating any two different dielectric media. Strictly speaking, each ϵ_{ij} and the first spatial derivatives thereof, being continuous across the limiting surface of any of those objects, must vary in a certain three-dimensional region containing those boundary surfaces. We suppose that the sizes (or transverse widths) of those regions in the directions orthogonal to the corresponding surfaces are adequately small. Except for the last assumptions regarding ϵ_{ij}, the formulation in this section is rather general, and it applies regardless of the fact that the objects are or are not identical cylindrical waveguides. The generalization of that three-dimensional formulation when ϵ_{ij} or the first spatial derivatives thereof are allowed to develop discontinuities at the boundaries of the dielectric objects, is rather complicated and it will not be attempted here. That generalization for electromagnetic scattering by optically anisotropic cylindrical waveguides, which becomes a two-dimensional situation, has already been carried out and reference to it will be given in Appendix E.

Let $\bar{\epsilon}(\bar{k}, \sigma)$ be the standard linear (real) or circular (complex) unit polarization vectors; they are given by the same expressions as for electromagnetic wave propagation in vacuum.[51] The (linear or circular) polarization index σ takes on only two values. Their basic properties are summarized in Appendix A. Let incoming classical monochromatic (complex) electric ($\mathbf{E}'_{in}\exp(-i\omega t)$) and magnetic ($\mathbf{H}'_{in}\exp(-i\omega t)$) fields, with real frequency ω and wavevector $\bar{k}$, propagate freely in the surrounding reference medium at very large distances from the N objects (say, for distances much larger than their characteristic sizes and larger than the wavelength). Certain shapes of the objects require specific discussions and treatments of what is meant by "distances much larger than their characteristic sizes." The case of cylindrical objects that have (relatively) large sizes along certain directions will be dealt with in Section 2.10. Both $\mathbf{E}'_{in}$ and $\mathbf{H}'_{in}$ fulfill Maxwell's equations (that is, Eqs. (2.1) and (2.2) with $\tilde{\epsilon} = I_3$). Then, both equations in (2.3) for $\mathbf{H}'_{in} = \mathbf{H}'_0 \exp i\bar{k}\bar{x}$, with constant $\mathbf{H}'_0$, read for any $\bar{x}$:

$$\nabla \times (\nabla \times \mathbf{H}'_{in}) = \frac{\omega^2}{v^2}\mathbf{H}'_{in}, \nabla \cdot \mathbf{H}'_{in} = 0 \tag{2.14}$$

The v now denotes the velocity of the electromagnetic wave in the surrounding reference medium. In general, $\mathbf{H}'_0$ is a linear combination of the two vectors $\bar{\epsilon}(\bar{k}, \sigma)$, for both values of σ. In order to simplify the analysis without an essential loss of generality, we choose $\mathbf{H}'_0 = \bar{\epsilon}(\bar{k}, \sigma_{in})$, with some given initial (linear or circular) polarization index σ_{in}. The first equation in (2.14) can be re-expressed using the second one as:

$$[\Delta + K_{cl}^2]\mathbf{H}'_{in} = 0, K_{cl}^2 = \frac{\omega^2}{v^2} \tag{2.15}$$

where $\Delta = \partial^2/\partial x_1^2 + \partial^2/\partial x_2^2 + \partial^2/\partial x_3^2$.

Let those incoming fields approach the anisotropic objects and be scattered by them. The total electric field ($\mathbf{E}'\exp(-i\omega t)$) equals the incoming plus the scattered field and so on for the total magnetic field ($\mathbf{H}'\exp(-i\omega t)$). Both $\mathbf{E}'$ and $\mathbf{H}'$ fulfill Maxwell's equations (2.1) and (2.2) for any $\bar{x}$ (in the surrounding reference medium and inside the objects). Notice that $\tilde{\epsilon} \neq I_3$ inside the objects. We shall concentrate on the total magnetic field that satisfies Eq. (2.3). For convenience, we shall recast Eq. (2.3) for $\mathbf{H}'$ at any $\bar{x}$ as:

$$[\Delta + K_{cl}^2]\mathbf{H}' = \mathbf{j}', \nabla \cdot \mathbf{H}' = 0 \tag{2.16}$$

$$\mathbf{j}' = \nabla \times ([(\tilde{\epsilon})^{-1} - I_3]\nabla \times \mathbf{H}') \tag{2.17}$$

It is easy to check that $\nabla \cdot \mathbf{j}' = 0$, so that Eq. (2.17) is consistent with the second Eq. (2.16). The structures of Eqs. (2.16) and (2.17) can be easily justified as follows. Let there be no anisotropic objects (ϵ_{ij} thereby becoming equal to δ_{ij}), so that the region of space occupied by them becomes similar to the surrounding reference medium. Then, there would be no scattered waves and, hence, $\mathbf{H}'$ would become $\mathbf{H}'_{in}$, $\mathbf{j}' = 0$ (the right-hand side of Eq. (2.17) vanishing identically) and the first Eq. (2.16) would become the first Eq. (2.15).

A Green's function ($G_{Tr}(\bar{x})$) adequate for dealing with both equations in (2.16) (and, specifically, for solving the difficulties arising from the second equation) has been proposed and adequately studied.[52,53] $G_{Tr}(\bar{x})$ is named the transverse Green's function and it is a 3×3 tensor, characterized in Appendix B. Upon applying standard Green's function techniques with $G_{Tr}(\bar{x} - \bar{x}')$, the partial differential equations in (2.16) can be recast as the following linear integral equation valid for any $\bar{x}$ (that is, both in the surrounding reference medium and inside any anisotropic object):

$$\mathbf{H}'(\bar{x}) = \mathbf{H}'_{in}(\bar{x}) + \int d^3\bar{x}' G_{Tr}(\bar{x} - \bar{x}')\mathbf{j}'(\bar{x}') \tag{2.18}$$

The integration over $\bar{x}'$ is extended to the whole regions occupied by the N separate optically anisotropic dielectric objects. Using the properties of $G_{Tr}(\bar{x})$, as outlined in Appendix B, one sees easily that $\mathbf{H}'(\bar{x})$, as given by the right-hand side of (2.18) fulfills, throughout all space, both the first (2.16) (for $\bar{x}$ inside the anisotropic objects and outside them) and the second (2.16). Eq. (2.18) is the basic integral equation describing the scattering of the classical electromagnetic wave by the separate optically anisotropic objects.

For $\mid \bar{x} \mid \rightarrow +\infty$, along a fixed direction (say, fixed $x_l / \mid \bar{x} \mid, l = 1, 2, 3$), by using Eq. (B.7), with $\bar{k}' = K_{cl}(\bar{x} / \mid \bar{x} \mid)$, Eq. (2.18) becomes:

$$\mathbf{H}'(\bar{x}) \rightarrow \mathbf{H}'_{in}(\bar{x}) + \frac{\exp i K_{cl} \mid \bar{x} \mid}{\mid \bar{x} \mid} \sum_{\sigma} \bar{\epsilon}(\bar{k}', \sigma) f(\bar{k}', \sigma; \bar{k}, \sigma_{in}) \tag{2.19}$$

$$f(\bar{k}', \sigma; \bar{k}, \sigma_{in}) = -\frac{1}{4\pi} \int d^3\bar{x}' \exp[-i\bar{k}'\bar{x}'] \bar{\epsilon}(\bar{k}', \sigma)^{+} \mathbf{j}'(\bar{x}') \tag{2.20}$$

The two $\bar{\epsilon}(\bar{k}', \sigma)$'s are also standard linear (real) or circular (complex) polarization vectors in three dimensions (see Appendix A). Recalling that $\mathbf{H}'_{in} = \bar{\epsilon}(\bar{k}, \sigma_{in}) \exp i\bar{k}\bar{x}$, we choose, for consistency, the $\bar{\epsilon}(\bar{k}', \sigma)$'s in (2.19) to represent the same type of polarization (linear or circular) as $\bar{\epsilon}(\bar{k}, \sigma_{in})$. The row vector $\bar{\epsilon}(\bar{k}', \sigma)^{+}$ is the adjoint (involving complex conjugation and matrix transposition) of the column vector $\bar{\epsilon}(\bar{k}', \sigma)$. Then, $\epsilon(\bar{k}, \sigma)^{+}\mathbf{j}'(\bar{x}')$ denotes the scalar product of the vector $\bar{\epsilon}(\bar{k}', \sigma)$ (involving the complex conjugate of its components) times $\mathbf{j}'(\bar{x}')$. The sum over the polarization index σ is carried out only over its two allowed values. $f(\bar{k}', \sigma; \bar{k}, \sigma_{in})$ is the three-dimensional electromagnetic scattering amplitude by the assembly of all anisotropic objects. See Figure 2.2.

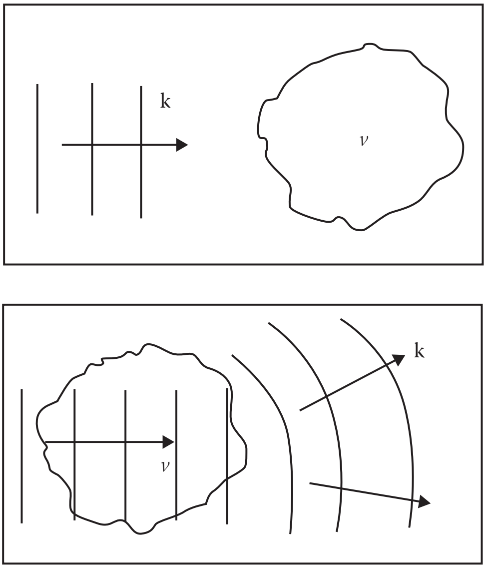

FIGURE 2.2 Top: Incoming electromagnetic radiation with wavevector $\bar{k}$ approaches an optically anisotropic three-dimensional object (V). Bottom: Scattered radiation by the optically anisotropic object in the direction corresponding to the outgoing wavevectors $\bar{k}'$.

Let us consider the flux of the Poynting vector determined by the incoming fields $\mathbf{E}'_{in}\exp(-i\omega t)$ and $\mathbf{H}'_{in}\exp(-i\omega t)$ (across a unit planar surface orthogonal to $\bar{k}$) and that corresponding to (2.19) and to its associated electric field (across a very small surface element orthogonal to $\bar{k}'$, located at $|\ \bar{x}\ |\to +\infty$). The ratio of the second flux over the first one yields the differential cross-section for the scattering by that assembly of anisotropic objects. That differential cross-section is proportional to $|\ f(\bar{k}', \sigma; \bar{k}, \sigma_{in})\ |^2$. We shall omit further details, as one may see similar computations elsewhere.[54]

Eq. (2.18) is a linear inhomogeneous integral equation that can be solved formally by successive iterations. The latter generate an infinite series for $\mathbf{H}'(\bar{x})$, which solves Eq. (2.18). For weak scattering processes, it suffices to approximate $\mathbf{H}'(\bar{x})$ by $\mathbf{H}'_{in}(\bar{x})$ plus the result of the first iteration. This yields the following approximate explicit representation for $\mathbf{H}'(\bar{x})$:

$$\mathbf{H}'(\bar{x}) \simeq \mathbf{H}'_{in}(\bar{x}) + \int d^3\bar{x}' G_{Tr}(\bar{x}-\bar{x}')\mathbf{j}'^{(1)}(\bar{x}') \tag{2.21}$$

$$\mathbf{j}'^{(1)}(\bar{x}') = \nabla \times ([(\tilde{\epsilon})^{-1} - I_3]\nabla \times \mathbf{H}'_{in}(\bar{x}')) \tag{2.22}$$

In this approximation (named the Debye-Born-Rayleigh-Gans or DBRG), $f(\bar{k}', \sigma; \bar{k}, \sigma_{in})$ is obtained by replacing $\mathbf{j}'(\bar{x}')$ in (2.20) by $\mathbf{j}'^{(1)}(\bar{x}')$:

$$\begin{aligned} f(\bar{k}', \sigma; \bar{k}, \sigma_{in}) &\simeq f(\bar{k}', \sigma; \bar{k}, \sigma_{in})_{DBRG} \\ &= -\frac{1}{4\pi}\int d^3\bar{x}' \exp[-i\bar{k}'\bar{x}']\bar{\epsilon}(\bar{k}', \sigma)^+ \mathbf{j}'^{(1)}(\bar{x}') \end{aligned} \tag{2.23}$$

Some necessary conditions for this approximation to hold are: i) $\tilde{\epsilon}$ differs little from I_3, that is, all $\mid \epsilon_{ii} - 1 \mid$ and all $\mid \epsilon_{ij} \mid$, $i \neq j$, are small compared to unity, and ii) all ϵ_{ij} vary slowly inside the objects. We shall leave the approximate explicit integral representation for $\mathbf{H}'(\bar{x})$ given by Eqs. (2.21) and (2.22) as it stands. In principle, it could be applied directly to some physically interesting scattering situations, say, through numerical integration. However, as we shall see, one may easily understand that its practical reliability would become reduced, at least, as the number of scattering objects increases; say, as the possibility of multiple scattering effects becomes non-negligible. That is, the above necessary conditions i) and ii) will not be sufficient for the reliability of (2.21) and (2.22) if the number of scattering objects is not adequately small.

Intuitively, one could imagine that the incoming field $\mathbf{H}'_{in}(\bar{x})$ is scattered once by each of the N anisotropic objects. Then, let the magnetic field arising from the scattering by the i-th anisotropic object alone be, in turn and subsequently, scattered by the j-th object ($j \neq i$) and so on. This gives rise to imagining a whole series of successive multiple scatterings of the electromagnetic wave by the different objects. At this stage, one could argue, quite naturally, that the exact total magnetic field $\mathbf{H}'(\bar{x})$, given by Eq. (2.18), should also be equal to the total magnetic field resulting from all those multiple scatterings. Such a multiple scattering point of view is physically correct and mathematically consistent, and it has given rise to further insight and useful approximations. Of course, the approximate (2.21) and (2.22) amount to neglecting all multiple scatterings (double, triple,. . .). So, *a posteriori*, we see that the approximate reliability of (2.21) and (2.22) would require that multiple scattering effects be adequately small, intuitively. The latter condition appears not to be fulfilled in many physically interesting cases (eventually not, if the number of scattering objects is adequately large).

Then, it makes sense to develop further alternative and general procedures that deal with multiple scattering specifically. A rather general formulation will be outlined in the next section. Its applicability (for N parallel cylindrical long waveguides) will be explained later in this chapter.

2.9 MULTIPLE SCATTERING BY OPTICALLY ANISOTROPIC OBJECTS IN THREE DIMENSIONS: AN OUTLINE

Let there be only one optically anisotropic object, namely, the i-th one (as if all the remaining $N - 1$ ones had been removed). Let $\mathbf{H}'(\bar{x})_i^{(a)}$ be the total magnetic field describing the scattering of the incoming field $\mathbf{H}'_{in}(\bar{x})$ by the i-th anisotropic object alone (superscript a). $\mathbf{H}'(\bar{x})_i^{(a)}$ fulfills Eq. (2.18) with only the i-th scattering object, which we cast as:

$$\mathbf{H}'(\bar{x})_i^{(a)} = \mathbf{H}'_{in}(\bar{x}) + \int_i d^3\bar{x}' G_{Tr}(\bar{x} - \bar{x}')\mathbf{j}'(\bar{x}')_i \tag{2.24}$$

$\mathbf{j}'(\bar{x}')_i$ is obtained from $\mathbf{j}'(\bar{x}')$ (Eq. (2.17)) upon replacing in it $\mathbf{H}'(\bar{x})$ by $\mathbf{H}'(\bar{x})_i^{(a)}$. The subscript i in the integral in Eq. (2.24) indicates that the integration over $\bar{x}'$ is extended only over the region occupied by the i-th object. The series for $\mathbf{H}'(\bar{x})_i^{(a)}$ formed by the all successive iterations of Eq. (2.24) can be recast symbolically as:

$$\mathbf{H}'_i(a) = \mathbf{H}'_{in} + G_{Tr}\tau_i\mathbf{H}'_{in} \tag{2.25}$$

Eq. (2.25) defines the scattering integral operator τ_i (which is also a 3×3 matrix) for the i-th object. More specifically, τ_i is given by a series, so that the n-th term in it is obtained from the n-th iteration of Eq. (2.24). For instance, the first iteration of Eq. (2.24) gives the first contribution, $\tau_i^{(1)}$, to τ_i ($\tau_i \simeq \tau_i^{(1)}$):

$$G_{Tr}\tau_i^{(1)}\mathbf{H}'_{in} = \int_i d^3\bar{x}' G_{Tr}(\bar{x} - \bar{x}')\mathbf{j}'^{(1)}(\bar{x}')_i \tag{2.26}$$

$\mathbf{j}'^{(1)}(\bar{x}')_i$ is given in (2.22) only for $\bar{x}'$ in the region occupied by the i-th scattering object. One can identify the explicit form of $\tau_i^{(1)}$ from (2.26) but, for brevity, we shall not write it (a similar identification will be carried out later in the simpler case of cylindrical waveguides). Similarly, the second iteration of Eq. (2.24) gives the second contribution, $\tau_i^{(2)}$, to τ_i ($\tau_i \simeq \tau_i^{(1)} + \tau_i^{(2)}$). In order to illustrate the potential usefulness of these studies, we note that the second iteration of (a far simpler version of) Eq. (2.24) was one key element in deriving the form birefringence coefficient for an array of parallel cylinders of arbitrary sizes and separations.[23] And so on for higher order contributions to τ_i. In the remainder of this section, we shall work with τ_i but no longer with $\mathbf{H}'(\bar{x})_i^{(a)}$.

Next, we again consider the case with all (N) optically anisotropic objects present and we treat all possible scatterings of the magnetic field by them. That is, we come back to the total magnetic field $\mathbf{H}'(\bar{x})$ describing the scattering of the incoming field $\mathbf{H}'_{in}(\bar{x})$ and to Eq. (2.18). The key features of the alternative multiple scattering formulation of Eq. (2.18) are the following. The same total magnetic field $\mathbf{H}'(\bar{x}) \equiv \mathbf{H}'$, which solves Eq. (2.18), is also given by the representation:

$$\mathbf{H}' = \mathbf{H}'_{in} + \sum_{i=1}^{N} G_{Tr}\tau_i\mathbf{H}'_i \tag{2.27}$$

In turn, the new "partial" magnetic fields $\mathbf{H}'_i = \mathbf{H}'(\bar{x})_i, i = 1, \ldots, N$, are the solution of the system:

$$\mathbf{H}'_i = \mathbf{H}'_{in} + \sum_{j=1, j\neq i}^{N} G_{Tr}\tau_j\mathbf{H}'_j \tag{2.28}$$

τ_i in both Eqs. (2.27) and (2.28) is the same as in Eq. (2.25), namely, the scattering integral operator for the i-th object. Eq. (2.28) is an inhomogeneous linear system of N integral equations for all $\mathbf{H}'_i$, $i = 1, \ldots, N$. Notice that the i-th Eq. (2.28) does not contain $\mathbf{H}'_i$ in its right-hand side. Physically, this can be interpreted through the statement that the magnetic field that reaches the i-th object is the sum of the incoming one plus the superposition of all those generated by the remaining $N - 1$ objects. We emphasize that $\mathbf{H}'(\bar{x})_i$ is physically different from $\mathbf{H}'(\bar{x})_i^{(a)}$ and it would be erroneous to confuse them; only the i-th object was present when $\mathbf{H}'(\bar{x})_i^{(a)}$ was defined (in Eq. (2.24), while all (N) objects were considered in Eq. (2.28) for $\mathbf{H}'(\bar{x})_i$. A key property is that the solution for $\mathbf{H}'$ obtained by all iterations of Eq. (2.28) together with Eq. (2.27) is equivalent to a rearrangement of the series obtained by iterating Eq. (2.18). It can be proved upon comparing the series formed by all successive iterations for Eq. (2.18) with the one provided by Eq. (2.27) and all successive iterations of Eq. (2.28).

The scattering amplitude $f(\bar{k}', \sigma; \bar{k}, \sigma_{in})$ ((2.17)) can be obtained, for instance, through the substitution of $\mathbf{H}'$ in (2.17) by the right-hand side of (2.27).

The multiple scattering formulation in quantum mechanics is well documented.[54–56] Its extension for the multiple scattering formulation of electromagnetic waves had to deal with the additional difficulties arising from the second equation in Eq. (2.16). The transverse Green's function G_{Tr} allowed us to solve those difficulties, as shown through further computations and estimates.[57]

In practice, the above multiple scattering formulation, although physically quite appealing, is not easy to apply, with the above generality, in three dimensions as the number N of scattering objects increases. Fortunately, the application of such formulation for parallel cylindrical waveguides (which boil down to treating two-dimensional situations) under additional simplifying assumptions will be more tractable, as we shall see. The rather general formulations in this and the preceding section could also provide some starting point for the study of electromagnetic wave scattering by objects, when those simplifying assumptions are not met with sufficient approximation (or are not fulfilled at all): for instance, for cylindrical waveguides with misalignments.

2.10 SCATTERING BY ANISOTROPIC CYLINDRICAL WAVEGUIDES

2.10.1 Two-Dimensional Maxwell's Equations for Anisotropic Cylindrical Waveguides

We shall now assume that each of the N objects is an optically anisotropic cylindrical waveguide with arbitrary transverse cross-section Ω and suitably large length L. Let R be some length scale so that the area of Ω is of order R^2. L is supposed to be much larger than R and than typical wavelengths of light, so, for practical purposes, the waveguide will be regarded to have infinite length ($L \simeq \infty$). See Figure 2.3. We suppose that all N waveguides have their axes parallel to one another. See Figure 2.4. We shall choose the x_3-axis to be parallel to the axis of the waveguides (for both $N = 1$ and $N > 1$) and write: $\bar{x} = (\boldsymbol{x}, x_3)$, so that $\boldsymbol{x} = (x_1, x_2)$. We shall suppose that $\epsilon_{13} = \epsilon_{23} = 0$, and that the non-vanishing ϵ_{ij} are real for typical frequencies of light, at least, approximately (absence of absorption). If, in addition, $\epsilon_{12} = \epsilon_{21} = 0$, the material of which the waveguide is made is, by definition, not optically active. Let a material be not optically active, then, the case $\epsilon_{11} = \epsilon_{22} \neq \epsilon_{33}$ corresponds to uniaxial anisotropy, while if all ϵ_{ii} differ from one another, one meets the biaxial one. In the general study that follows, and unless explicitly stated, we shall allow for optically active materials ($\epsilon_{12} = \epsilon_{21} \neq 0$).

Under the above additional simplifications, the general three-dimensional scattering problem treated in Section 2.8 can be reduced to a somewhat simpler one, in two spatial dimensions. In fact, with $L \simeq +\infty$, it is consistent to search for

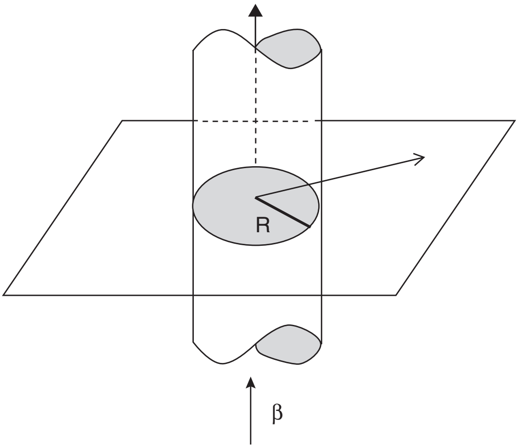

FIGURE 2.3 One single anisotropic object having the form of a cylindrical waveguide of radius R. The constant β appearing in Eq. (2.30) is displayed. β also gives the component of the wavevector of the incoming radiation parallel to the axis of the waveguide.

physically consistent solutions of Maxwell's equations, in which the x_3-dependences are factorized in the total electric and magnetic fields:

$$\mathbf{E}' = \exp(i\beta x_3)\mathbf{E} \tag{2.29}$$

$$\mathbf{H}' = \exp(i\beta x_3)\mathbf{H} \tag{2.30}$$

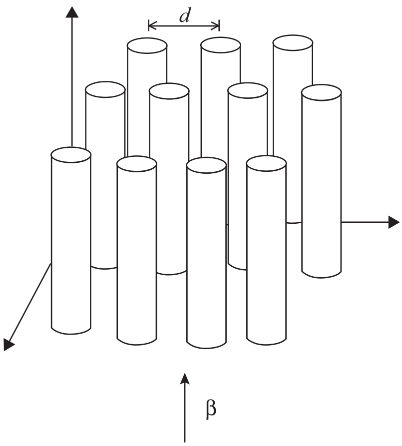

FIGURE 2.4 N anisotropic objects, each having the form of a cylindrical waveguide. The axes of the N waveguides are parallel to one another. The average distance between any pair of neighboring waveguides is d. The constant β appearing in Eq. (2.30) is displayed (see also caption of Figure 2.3). For comparison with Figure 2.6, the optic axis of each waveguide is supposed to be parallel to its geometric axis.

Both **E** and **H** are independent on x_3, but they do depend on $\boldsymbol{x} = (x_1, x_2)$. On the other hand, β is a real constant (as absorption effects are regarded as negligible).

Let $\mathbf{E} = (E_1, E_2, E_3)$ and $\mathbf{H} = (H_1, H_2, H_3)$. In this case, we shall give a simpler (two-dimensional) form of Maxwell's equations, involving only H_1 and H_2. Such a form will turn out to be equivalent to the two equations in (2.3) plus Eq. (2.30). For that purpose, one could use Eq. (2.3), as we shall comment in Appendix C, but we shall proceed through an alternative route. Thus, we consider the first components of the first (vector) equation in (2.2) and the third component in the first (also vector) equation in (2.1) and take Eq. (2.29) into account. All those yield:

$$\frac{\partial H_2}{\partial x_1} - \frac{\partial H_1}{\partial x_2} = -\frac{i\omega}{v}\left(\frac{\epsilon_0}{\mu_0}\right)^{1/2} \epsilon_{33} E_3 \tag{2.31}$$

$$\frac{\partial E_3}{\partial x_2} - i\beta E_2 = \frac{i\omega}{v}\left(\frac{\mu_0}{\epsilon_0}\right)^{1/2} H_1, \quad -\frac{\partial E_3}{\partial x_1} + i\beta E_1 = \frac{i\omega}{v}(\frac{\mu_0}{\epsilon_0})^{1/2} H_2 \tag{2.32}$$

Eqs. (2.31) and (2.32) allow us to obtain, successively, E_3 and, then, E_2 and E_1 in terms of H_1 and H_2. Then, we consider $\nabla \times (\nabla \times \mathbf{H}') = -i(\omega/v)(\epsilon_0/\mu_0)^{1/2} \nabla \times (\epsilon \mathbf{E}')$, take its first two components, use the second equation in (2.2) and Eq. (2.30) and employ the above expressions for E_3, E_2 and E_1 in terms of H_1 and H_2 and spatial derivatives thereof. Thus, one finds the announced system depending only on H_1 and H_2 (with $\Delta_T \equiv \partial^2/\partial x_1^2 + \partial^2/\partial x_2^2$ and $K^2 = (\omega/v)^2 - \beta^2$):

$$[\Delta_T + K^2]H_i = j_i, \quad i = 1, 2 \tag{2.33}$$

$$j_1 = -(\omega/v)^2(\epsilon_{22} - 1)H_1 + (\omega/v)^2 \epsilon_{21} H_2 - \frac{\partial \ln \epsilon_{33}}{\partial x_2}\left[\frac{\partial H_2}{\partial x_1} - \frac{\partial H_1}{\partial x_2}\right]$$
$$+ \left(\epsilon_{21}\frac{\partial}{\partial x_1} - (\epsilon_{33} - \epsilon_{22})\frac{\partial}{\partial x_2}\right)\left[\frac{1}{\epsilon_{33}}\left(\frac{\partial H_2}{\partial x_1} - \frac{\partial H_1}{\partial x_2}\right)\right] \tag{2.34}$$

$$j_2 = -(\omega/v)^2(\epsilon_{11} - 1)H_2 + (\omega/v)^2 \epsilon_{12} H_1 + \frac{\partial \ln \epsilon_{33}}{\partial x_1}\left[\frac{\partial H_2}{\partial x_1} - \frac{\partial H_1}{\partial x_2}\right]$$
$$- \left(\epsilon_{12}\frac{\partial}{\partial x_2} - (\epsilon_{33} - \epsilon_{11})\frac{\partial}{\partial x_1}\right)\left[\frac{1}{\epsilon_{33}}\left(\frac{\partial H_2}{\partial x_1} - \frac{\partial H_1}{\partial x_2}\right)\right] \tag{2.35}$$

for any $\boldsymbol{x}$. Both j_1 and j_2 vanish outside the transverse cross-section of any anisotropic waveguide. A distinguishing feature of (2.34) and (2.35) is that the components of $\tilde{\epsilon}^{-1}$ do not appear explicitly in them. Notice that the above Eqs. (2.34) and (2.35) correct for a sign missprint in a previous work[19] (specifically, in the second term on the right-hand side of Eq. (2.1.8) in that work.[19]) Eqs. (2.33), (2.34) and (2.35) hold independently on any assumption about the behavior of the components of $\tilde{\epsilon}$ and their first spatial derivatives across any interface between the cylindrical waveguides and the surrounding medium (cladding).

In turn, Eqs. (2.33), (2.34) and (2.35) can be recast as

$$[\Delta_T + K^2]h(\boldsymbol{x}) = j(\boldsymbol{x}) \tag{2.36}$$

where $h = h(\boldsymbol{x})$ and $j = j(\boldsymbol{x})$ are the two column vectors formed, respectively, by $H_i, i = 1, 2$ and by $j_i, i = 1, 2$.

In what follows, and in order to simplify the analysis, we shall suppose that $\epsilon_{ij}, i, j = 1, 2, \epsilon_{33}$ and their first spatial derivatives are continuous throughout all space (that is, and in particular, also across any interface separating any anisotropic waveguide and the surrounding cladding). This is the counterpart for the actual cylindrical waveguides of similar assumptions for the three-dimensional case made in Section 2.8.

2.10.2 Scattering by N Anisotropic Cylindrical Waveguides: General Analysis

Let $H_0^{(1)}(K \mid \boldsymbol{x} \mid)$ be Hankel's outgoing function of zeroth order.[58] It fulfills:

$$[\Delta_T + K^2]\frac{H_0^{(1)}(K \mid \boldsymbol{x} - \boldsymbol{x}' \mid)}{4i} = \delta^{(2)}(\boldsymbol{x} - \boldsymbol{x}') \tag{2.37}$$

$\delta^{(2)}$ being the two-dimensional Dirac delta function. That is, $H_0^{(1)}(K \mid \boldsymbol{x} - \boldsymbol{x}' \mid)/4i$ is a Green's function for $\Delta_T + K^2$, in two spatial dimensions. Some useful properties of $H_0^{(1)}(K \mid \boldsymbol{x} \mid)$ are collected in Appendix D. For the general case of N cylindrical waveguides, and upon applying standard Green's function techniques, the partial differential equation (2.36) can be recast as the following linear integral equation

$$h(\boldsymbol{x}) = h^{(0)}(\boldsymbol{x}) + \int d^2\boldsymbol{x}'\frac{H_0^{(1)}(K \mid \boldsymbol{x} - \boldsymbol{x}' \mid)}{4i} j(\boldsymbol{x}') \tag{2.38}$$

The integral in Eq. (2.38) is extended over the transverse cross-sections of the N anisotropic waveguides. The inhomogeneous term $h^{(0)}(\boldsymbol{x})$ fulfills $[\Delta_T + K^2]h^{(0)}(\boldsymbol{x}) = 0$ for any $\boldsymbol{x}$. For the scattering situation, there certainly is one physically propagating wave very far from the waveguide, namely the incoming plane wave: in this case, $h^{(0)}(\boldsymbol{x}) = h^{(0)} \exp i\boldsymbol{x}\boldsymbol{k}$, with $\boldsymbol{k}^2 = K^2 > 0$, that is, K is real. On the other hand, $h^{(0)}$ is $\boldsymbol{x}$-independent. Without an essential loss of generality, we can choose $h^{(0)}$ to equal a two-component linear (real) or circular (complex) polarization vector $\epsilon(\boldsymbol{k}, \sigma_{in})$ in two dimensions (see Appendix D). σ_{in} denotes the initial (linear or circular) polarization index. The three-dimensional Eq. (2.18) has simplified to the two-dimensional Eq. (2.38). $h^{(0)}(\boldsymbol{x})$ in (2.38) is the present two-dimensional counterpart of $\mathbf{H}'_{in}$ for (2.18).

For $\mid \boldsymbol{x} \mid \to +\infty$, along a fixed direction (say, fixed $x_l / \mid \boldsymbol{x} \mid, l = 1, 2$), and with $\boldsymbol{k}' \equiv K(\boldsymbol{x}/ \mid \boldsymbol{x} \mid)$, Eqs. (2.38) and (D.2) lead to:

$$h(\boldsymbol{x}) \to h^{(0)}(\boldsymbol{x}) + \frac{\exp iK \mid \boldsymbol{x} \mid}{\mid \boldsymbol{x} \mid^{1/2}} \sum_{\sigma} f_w(\boldsymbol{k}', \sigma; \boldsymbol{k}, \sigma_{in})\epsilon(\boldsymbol{k}', \sigma) \tag{2.39}$$

$$f_w(\boldsymbol{k}', \sigma; \boldsymbol{k}, \sigma_{in}) = \frac{1}{4i}\left[\frac{2}{\pi K}\right]^{1/2} \exp[-i\pi/4]\int d^2\boldsymbol{x}' \exp[-i\boldsymbol{k}'\boldsymbol{x}']\epsilon(\boldsymbol{k}', \sigma)^+ j(\boldsymbol{x}') \tag{2.40}$$

$\epsilon(\boldsymbol{k}', \sigma)$ is a possible two-component linear (real) or circular (complex) polarization vector in two dimensions (Appendix D). The sum over the polarization index σ is carried over only two values. $f_w(\boldsymbol{k}', \sigma; \boldsymbol{k}, \sigma_{in})$ is the two-dimensional electromagnetic scattering amplitude by the N anisotropic cylindrical waveguides.

Eq. (2.38) also applies for confined propagation (with $h^{(0)}(\boldsymbol{x}) = 0$ and K pure imaginary); Section 2.12 will be devoted to studying that physical situation.

2.10.3 One Anisotropic Cylindrical Waveguide: Weak Scattering

We now restrict the study in the precedent subsection to the case of only one cylindrical waveguide (all the remaining $N - 1$ ones being removed by assumption). We concentrate on Eq. (2.38), when the integral in it refers only to that unique waveguide.

Notice that $h(\boldsymbol{x}')$ and derivatives thereof appear inside $j(\boldsymbol{x}')$ (as implied by Eqs. (2.34) and (2.35)). It is possible to recast Eq. (2.38) into an equivalent form in which only $h(\boldsymbol{x}')$ (but not its derivatives) appears inside the integral over $\boldsymbol{x}'$. This is at the expense of having derivatives of $H_0^{(1)}(K \mid \boldsymbol{x} - \boldsymbol{x}' \mid)$ inside that integral. The alternative form of Eq. (2.38) is commented succinctly in Appendix E and has been treated in detail previously.[19]

If the anisotropic waveguide is a weak scatterer (say, if all $\mid \epsilon_{ii} - 1 \mid$ and $\mid \epsilon_{12} \mid$ are small compared to unity), it suffices to approximate $h(\boldsymbol{x})$ by $h^{(0)}(\boldsymbol{x})$ plus the result of the first iteration of Eq. (2.38). One gets:

$$h(\boldsymbol{x}) \simeq h^{(0)}(\boldsymbol{x}) + \int d^2\boldsymbol{x}' \frac{H_0^{(1)}(K \mid \boldsymbol{x} - \boldsymbol{x}' \mid)}{4i} j^{(1)}(\boldsymbol{x}') \tag{2.41}$$

where $j^{(1)}(\boldsymbol{x}')$ is obtained upon replacing $h(\boldsymbol{x}')$ by $h^{(0)}(\boldsymbol{x}')$ in $j(\boldsymbol{x}')$ (notice that a similar procedure was employed in Eqs. (2.21) and (2.22)). The integral in the right-hand side of Eq. (2.41) is extended only over the transverse cross-section of the unique waveguide considered here. In turn, the replacement of $h(\boldsymbol{x}')$ by $h^{(0)}(\boldsymbol{x}')$ in Eq. (2.40) provides the Debye-Born-Rayleigh-Gans approximation $f_w(\boldsymbol{k}', \sigma; \boldsymbol{k}, \sigma_{in})_{DBRG}$ for $f_w(\boldsymbol{k}', \sigma; \boldsymbol{k}, \sigma_{in})$:

$$\begin{aligned} f_w(\boldsymbol{k}', \sigma; \boldsymbol{k}, \sigma_{in})_{DBRG} &= \frac{1}{4i} \left[\frac{2}{\pi K}\right]^{1/2} \exp[-i\pi/4] \\ &\cdot \int d^2\boldsymbol{x}' \exp[-i\boldsymbol{k}'\boldsymbol{x}'] \epsilon(\boldsymbol{k}', \sigma)^{+} j^{(1)}(\boldsymbol{x}') \end{aligned} \tag{2.42}$$

In previous works,[20,31] the scattering by one anisotropic waveguide has been studied using Eq. (2.41) and a detailed numerical analysis. In those works, the following useful and practical conclusions have been reached for weak scattering. Let: i) ϵ_{12} and $\epsilon_{11} - \epsilon_{22}$ be suitably small (say, small optical activity and anisotropic waveguide relatively close to uniaxial behavior), ii) ϵ_{11} and ϵ_{33} be weakly dependent on $\boldsymbol{x}$, and iii) let $\boldsymbol{k}$ be suitably small, so that $h^{(0)}(\boldsymbol{x}')$ varies little as $\boldsymbol{x}'$ does inside the transverse section of the waveguide. Then, the contribution of $j^{(1)}(\boldsymbol{x}')$ to the integral in (2.41) is dominated by the terms independent on spatial derivatives of $H_0^{(1)}(K \mid \boldsymbol{x} - \boldsymbol{x}' \mid)$.[20,31]

2.10.4 Scattering by One Anisotropic Cylindrical Waveguide: Long Wavelength Approximation

We shall now outline a long-wavelength approximation for the scattering by one waveguide. Besides the above weak scatterer assumptions in the previous subsection, let us suppose that K (real) is such that the dimensionless product $\mid K \mid R$ is smaller than unity (the area of the transverse cross-section Ω of the cylindrical waveguide being of order R^2). Consistently with the last assumption, we neglect the $\boldsymbol{x}'$ dependence in $h(\boldsymbol{x}')$ inside the integral, as we integrate over $\boldsymbol{x}'$ with $\mid \boldsymbol{x}' \mid$ less than about R. Also, we shall restrict to $\boldsymbol{x}$ such that $\mid K \mid\mid \boldsymbol{x} \mid \leq 1$. Then $h^{(0)}(\boldsymbol{y}) = h^{(0)} \exp i\boldsymbol{yk} \simeq h^{(0)}$ for $\boldsymbol{y} = \boldsymbol{x}$, and $\boldsymbol{x}'$. Also, $h = h(\boldsymbol{x})$ is essentially independent on $\boldsymbol{x}$, and we also denote its two constant components by H_i, $i = 1, 2$. One can apply the approximation (D.5) to the integral in the second term of the right-hand side of the exact Eq. (2.38) (but, in principle, not to that of the first-order correction to Eq. (2.38), given in Eq. (2.41)). Then:

$$h \simeq h^{(0)} + \frac{1}{2\pi} \ln[-2^{-1} i K R \exp\gamma] \int d^2\boldsymbol{x}' j(\boldsymbol{x}') \tag{2.43}$$

γ being Euler's constant.[58] In turn, as we have neglected the $\boldsymbol{x}'$ dependence of h inside the integral, one has $\partial H_i/\partial x_j = 0$ for $i, j = 1, 2$, and the two components of the actual $j(\boldsymbol{x}')$ in (2.43) reduce to:

$$j(\boldsymbol{x}')_1 = \left(\frac{\omega}{v}\right)^2 [-(\epsilon_{22}(\boldsymbol{x}') - 1)H_1 + \epsilon_{21}(\boldsymbol{x}')H_2] \equiv \sum_{j=1}^{2} (A_2(\boldsymbol{x}'))_{1j} H_j \tag{2.44}$$

$$j(\boldsymbol{x}')_2 = \left(\frac{\omega}{v}\right)^2 [-(\epsilon_{11}(\boldsymbol{x}') - 1)H_2 + \epsilon_{12}(\boldsymbol{x}')H_1] \equiv \sum_{j=1}^{2} (A_2(\boldsymbol{x}'))_{2j} H_j \tag{2.45}$$

The right-hand sides of (2.44) and (2.45) define the four elements $(A_2(\boldsymbol{x}'))_{ij}$ of the 2×2 matrix $A_2(\boldsymbol{x}')$. The notation indicates the fact that ϵ_{ij} may still depend on $\boldsymbol{x}'$. Eq. (2.43) should not be confused with Eq. (2.41). Thus, Eq. (2.41) requires weak scattering and includes only the first iteration, but it is not restricted to long wavelength. On the other hand, Eq. (2.43) requires weak scattering as well, but it amounts to treating approximately all iterations of Eq. (2.38), although it is restricted to long wavelength. Thus, even if, for physical consistency, the weak scatterer assumptions are also involved in Eq. (2.43), all higher order iterations of Eq. (2.38)) are to be taken into account in the approximation. Eq. (2.43) is an inhomogeneous linear system of two equations for H_i, $i = 1, 2$ that can be trivially solved and so provides the basis for an explicit approximate solution valid for long wavelength scattering. One gets:

$$h \simeq [I_2 - (2\pi)^{-1} \ln(-2^{-1} i K R \exp\gamma) A_2]^{-1} h^{(0)} \tag{2.46}$$

$$A_2 \equiv \int d^2\boldsymbol{x}' A_2(\boldsymbol{x}') \tag{2.47}$$

I_2 is the 2×2 unit matrix. Notice that $[I_2 - (2\pi)^{-1} \ln(-2^{-1} i K R \exp\gamma) A_2]^{-1}$ is a 2×2 matrix.

Using Eqs. (2.40) and (2.46), the scattering amplitude in the long wavelength approximation reads:

$$f_w(\mathbf{k}', \sigma; \mathbf{k}, \sigma_{in}) \simeq \frac{1}{4i} \exp[-i\pi/4] \left[\frac{2}{\pi K}\right]^{1/2}$$
$$\times\, \epsilon(\mathbf{k}', \sigma)^{+} A_2[I_2 - (2\pi)^{-1} \ln(-2^{-1} i K R \exp\gamma) A_2]^{-1} h^{(0)} \quad (2.48)$$

The well known optical theorem,[54,56] is a general consistency requirement that must be satisfied by the scattering amplitude. It is easy to see that the long wavelength approximation given in Eq. (2.48) satisfies approximately the optical theorem. For brevity, we shall omit details.

2.10.5 Multiple Scattering by N Parallel Anisotropic Waveguides: Approximations

With a view toward the analysis of the interaction of light with N parallel optically anisotropic cylindrical waveguides and a multiple scattering formulation thereof (restricting the general three-dimensional approach outlined in Section 2.9 to the actual two-dimensional case), we shall start with the case of only one cylindrical waveguide (all the remaining $N-1$ ones being removed for the time being). Then, we consider Eq. (2.38) for only one cylindrical waveguide. We notice that the series for $h(\mathbf{x})$ formed by the all successive iterations of Eq. (2.38) (providing its solution for one waveguide) can be rewritten formally as follows. By omitting explicit $\mathbf{x}$ dependences, such a series solution of Eq. (2.38) can be cast as:

$$h = h^{(0)} + \frac{H_0^{(1)}}{4i} \tau_w h^{(0)} \quad (2.49)$$

which defines the waveguide scattering integral operator τ_w (which is also a 2×2 matrix). In detail, Eq. (2.49) reads:

$$h(\mathbf{x}) = h^{(0)}(\mathbf{x}) + \int d^2\mathbf{x}' \int d^2\mathbf{x}'' \frac{H_0^{(1)}(K \mid \mathbf{x} - \mathbf{x}' \mid)}{4i} \tau_w(\mathbf{x}', \mathbf{x}'') h^{(0)}(\mathbf{x}'') \quad (2.50)$$

The integrations over both $\mathbf{x}'$ and $\mathbf{x}''$ in (2.50) are carried out over the transverse cross-section of the waveguide. The comparison between the exact Eq. (2.50) and the approximate Eq. (2.41) would allow us to characterize the first approximation $\tau_w^{(1)}$ for τ_w. One has:

$$\int d^2\mathbf{x}'' \tau_w^{(1)}(\mathbf{x}', \mathbf{x}'') h^{(0)}(\mathbf{x}'') = j^{(1)}(\mathbf{x}') \quad (2.51)$$

$\tau_w^{(1)}(\mathbf{x}', \mathbf{x}'')$ could be inferred from the validity of Eq. (2.51) for any $h^{(0)}$. We shall not pursue this and we shall now give an explicit long wavelength approximation for τ_w, based upon the previous subsection. Thus, under the long wavelength approximation (so that both h and $h^{(0)}$ are $\mathbf{x}$-independent), the comparison between (2.50) and (2.46) yields an explicit approximation, $\int d^2\boldsymbol{x}' \int d^2\boldsymbol{x}''\tau_{w,lw}$, for the double integral $\int d^2\boldsymbol{x}' \int d^2\boldsymbol{x}''\tau_w$:

$$\int d^2\boldsymbol{x}' \int d^2\boldsymbol{x}''\tau_{w,lw}(\boldsymbol{x}', \boldsymbol{x}'') \\ = A_2[I_2 - (2\pi)^{-1}\ln(-2^{-1}iKR\exp\gamma)A_2]^{-1} \tag{2.52}$$

We now come back to the scattering of the incoming field $h^{(0)}(\boldsymbol{x})$ by all (N) parallel anisotropic cylindrical waveguides, by restricting to two dimensions the three-dimensional multiple scattering approach outlined in Section 2.9. Neither weak scatterer nor long wavelength approximations will be made, unless otherwise stated. In such an application, an important additional simplification occurs: one no longer works with the more complicated transverse Green's function G_{Tr} but with the simpler Green's function $H_0^{(1)}/4i$.

We shall also have in mind Eqs. (2.38) and (2.49) for each single waveguide: they characterize the waveguide scattering (2×2 matrix) integral operator $\tau_{w,i}$ ($= \tau_{w,i}(\boldsymbol{x}', \boldsymbol{x}'')$) for the i-th anisotropic waveguide. Let $h(\boldsymbol{x})$ be the total magnetic field describing the scattering of the incoming field $h^{(0)}(\boldsymbol{x})$ by the N waveguides: $h(\boldsymbol{x}) \equiv h$ (which is a column vector with two components) fulfills Eq. (2.38), the integration over $\boldsymbol{x}'$ being extended over the N transverse cross-sections of the waveguides. In the multiple scattering formulation, the same total magnetic field h, is also given by:

$$h = h^{(0)} + \sum_{i=1}^{N} \frac{H_0^{(1)}}{4i}\tau_{w,i}h_i \tag{2.53}$$

In turn, the new "partial" magnetic fields $h_i = h_i(\boldsymbol{x}), i = 1, \ldots, N$, are the solution of:

$$h_i = h^{(0)} + \sum_{j=1, j\neq i}^{N} \frac{H_0^{(1)}}{4i}\tau_{w,j}h_j \tag{2.54}$$

Eq. (2.54) is an inhomogeneous linear system of N integral equations for all h_j, $j = 1, \ldots, N$. Recall that each h_j is a column vector with two components. At this stage, we take the long distance limit in Eq. (2.53) ($\mid \boldsymbol{x} \mid \rightarrow +\infty$, along a fixed direction, with $\boldsymbol{k}' \equiv K(\boldsymbol{x}/ \mid \boldsymbol{x} \mid)$) and recall Eq. (D.2). One gets again Eq. (2.39), with an alternative representation for the scattering amplitude $f_w(\boldsymbol{k}', \sigma; \boldsymbol{k}, \sigma_{in})$ in terms of all h_i, namely:

$$f_w(\boldsymbol{k}', \sigma; \boldsymbol{k}, \sigma_{in}) = \frac{1}{4i}\left[\frac{2}{\pi K}\right]^{1/2} \exp[-i\pi/4] \sum_{i=1}^{N} \int d^2\boldsymbol{x}' d^2\boldsymbol{x}'' \exp[-i\boldsymbol{k}'\boldsymbol{x}'] \\ \times \epsilon(\boldsymbol{k}', \sigma)^+ \tau_{w,i}(\boldsymbol{x}', \boldsymbol{x}'')h_i(\boldsymbol{x}') \tag{2.55}$$

We emphasize that no approximations are involved in either Eq. (2.53) or Eq. (2.54). We shall turn to perform approximations on them in the remainder of this subsection and in the following one.

Let us choose some fixed axis inside the i-th cylindrical waveguide and another one in the j-th one ($i \neq j$), both of them being parallel to the x_3 axis. Let $D_{ij}, i \neq j$, be the distance between those two axes (measured, of course, in a plane orthogonal to the x_3 axis). D_{ij} gives information about the average separation between those waveguides. In various cases of physical interest, like several that apply to biological waveguides in the eye (Section 2.7), D_{ij}, R (the typical transverse dimension of any waveguide) and the typical wavelengths of light have about similar orders of magnitude. Then, Eq. (2.54) is not easy to analyze and one may have to turn to numerical studies directly.

Certain cases, in which some length parameters are larger than the others, become more tractable from the theoretical point of view, as we shall see. Let us suppose that all D_{ij} are adequately larger than R (the typical transverse dimension of any waveguide) and than $2\pi K^{-1}$ (the wavelength of light). Let $\boldsymbol{x}$ lie inside the transverse cross-section of any of the N waveguides. Then, we replace, at least formally, all $H_0^{(1)}/4i$ in Eq. (2.54) by their large separation approximation, as given in (D.6). Thus, Eq. (2.54) becomes:

$$h_i(\boldsymbol{x}) \simeq h^{(0)}(\boldsymbol{x}) + \sum_{j=1, j\neq i}^{N} \frac{1}{4i}\left[\frac{2}{\pi K D_{ij}}\right]^{1/2} \exp i(K D_{ij} - \pi/4)$$
$$\times \exp[i K \boldsymbol{u}_{ij}(\boldsymbol{x} - \boldsymbol{z}_i)] Y_j(\boldsymbol{u}_{ij}) \tag{2.56}$$

$$Y_j(\boldsymbol{u}_{ij}) \equiv \int d^2\boldsymbol{x}' \int d^2\boldsymbol{x}'' \exp[-i K \boldsymbol{u}_{ij}(\boldsymbol{x}' - \boldsymbol{z}_j)] \tau_{w,j}(\boldsymbol{x}', \boldsymbol{x}'') h_j(\boldsymbol{x}'') \tag{2.57}$$

The integrations over both $\boldsymbol{x}'$ and $\boldsymbol{x}''$ in (2.57) are carried out over the transverse cross-section of the j-th waveguide. Notice the key feature that all $Y_j(\boldsymbol{u}_{ij})$ are column vectors with two ($\boldsymbol{x}$-independent but $\boldsymbol{u}_{ij}$-dependent) components. Next, we consider (2.56) for $i = 1$ and $\boldsymbol{x}$ lying inside the transverse cross-section of that first waveguide and we multiply, successively, that equation by $\exp[-i K \boldsymbol{u}_{s1}(\boldsymbol{x}''' - z_1)]\tau_{w,1}(\boldsymbol{x}''', \boldsymbol{x})$, with $s = 2, \ldots N$. This gives rise to $N-1$ separate equations, for the different values of s. In each of the $N-1$ equations so resulting, we integrate the above products over both $\boldsymbol{x}'''$ and $\boldsymbol{x}$ inside the transverse cross-section of the first cylindrical waveguide. Then, the left-hand sides of the resulting $N-1$ equations become $Y_1(\boldsymbol{u}_{s1})$. We perform similar operations successively with (2.56) for $i = 2, \ldots N$ and $\boldsymbol{x}$ lying, in each case, inside the transverse cross-section of that i-th waveguide. Then, (2.56) becomes an inhomogeneous linear and purely algebraic system for all $Y_i(\boldsymbol{u}_{si})$, $s \neq i$:

$$Y_i(\boldsymbol{u}_{si}) = Y_i^{(0)}(\boldsymbol{u}_{si}) + \sum_{j=1, j\neq i}^{N} \Lambda_{i,j}(\boldsymbol{u}_{si}, \boldsymbol{u}_{ij}) Y_j(\boldsymbol{u}_{ij}) \tag{2.58}$$

where:

$$Y_i^{(0)}(\boldsymbol{u}_{si}) = \int d^2\boldsymbol{x}''' \int d^2\boldsymbol{x}_i \exp[-i K \boldsymbol{u}_{si}(\boldsymbol{x}''' - z_i)] \tau_{w,i}(\boldsymbol{x}''', \boldsymbol{x}) h^{(0)}(\boldsymbol{x}) \tag{2.59}$$

$$\Lambda_{i,j}(\boldsymbol{u}_{si}, \boldsymbol{u}_{ij}) = \frac{1}{4i}\left[\frac{2}{\pi K D_{ij}}\right]^{1/2} \exp i(K D_{ij} - \pi/4) \int d^2\boldsymbol{x}''' \int d^2\boldsymbol{x}$$
$$\times \exp[-i K \boldsymbol{u}_{si}(\boldsymbol{x}''' - z_i)] \tau_{w,i}(\boldsymbol{x}''', \boldsymbol{x}) \exp[i K \boldsymbol{u}_{ij}(\boldsymbol{x} - z_i)] \tag{2.60}$$

All $Y_j^{(0)}(\boldsymbol{u}_{si})$ are column vectors with two $\boldsymbol{x}$-independent components, while each $\Lambda_{ij}(\boldsymbol{u}_{si}, \boldsymbol{u}_{ij})$ is a 2×2 matrix with four $\boldsymbol{x}$-independent components.

To summarize: all $Y_i(\boldsymbol{u}_{si})$, $s \neq i$, are given by solving the inhomogeneous algebraic system (2.58). Then, Eq. (2.56) provides $h_i(\boldsymbol{x})$ for $\boldsymbol{x}$ inside the i-th waveguide. Finally, Eq. (2.55) gives the scattering amplitude in terms of all $h_i(\boldsymbol{x})$, as $\boldsymbol{x}$ varies inside the i-th waveguide. Then, when all D_{ij} are suitably large, the solution of the multiple scattering of an electromagnetic wave by N parallel anisotropic cylindrical waveguides is, in essence, reduced to the explicit knowledge of suitable integrals of all $\tau_{w,i}(\boldsymbol{x}''', \boldsymbol{x})$ and to the solution of an inhomogeneous system of algebraic system (for all $Y_i(\boldsymbol{u}_{si})$, $s \neq i$). $\tau_{w,i}(\boldsymbol{x}''', \boldsymbol{x})$ are discussed further below.

In general, there still remain the difficulties involved in the computations of integrals of all $\tau_{w,i}(\boldsymbol{x}''', \boldsymbol{x})$, which, in particular, are required in order to know the constant column vectors $Y_i^{(0)}(\boldsymbol{u}_{si})$ and the constant 2×2 matrices $\Lambda_{i,j}(\boldsymbol{u}_{si}, \boldsymbol{u}_{ij})$. One could proceed further, upon replacing each $\tau_{w,i}$ by its first approximation $\tau_w^{(1)}$, characterized previously in this subsection. Another possibility consists in applying the long wavelength approximation, to which we now turn. As not only all D_{ij} are large but the wavelength is also large, we have to be more specific about their relative magnitudes. For the validity of the approximate equations below, we shall suppose that all separations are larger than the wavelength which, in turn, is larger than the typical transverse sizes of all waveguides: $D_{ij} > 2\pi K^{-1} > R$. Then, upon integrating inside the transverse cross-section of each cylindrical waveguide in Eqs. (2.59), (2.60), $h^{(0)}(\boldsymbol{x})$ can be regarded as approximately constant and all K-dependent exponentials can be approximated by unity. The new simplifying feature is that Eq. (2.52) can now be applied for each waveguide. Then, Eqs. (2.59) and (2.60) become:

$$Y_i^{(0)}(\boldsymbol{u}_{si}) \simeq \int d^2\boldsymbol{x}''' \int d^2\boldsymbol{x}\, \tau_{w,i}(\boldsymbol{x}''', \boldsymbol{x}) h^{(0)} \tag{2.61}$$

$$\Lambda_{i,j}(\boldsymbol{u}_{si}, \boldsymbol{u}_{ij}) \simeq \frac{1}{4i}\left[\frac{2}{\pi K D_{ij}}\right]^{1/2} \exp i(K D_{ij} - \pi/4)$$
$$\times \int d^2\boldsymbol{x}''' \int d^2\boldsymbol{x}\, \tau_{w,i}(\boldsymbol{x}''', \boldsymbol{x}) \tag{2.62}$$

The double integral $\int d^2\boldsymbol{x}' \int d^2\boldsymbol{x}'' \tau_{w,i}(\boldsymbol{x}', \boldsymbol{x}'')$ (a constant 2×2 matrix) is given by the right-hand side of (2.52) for each waveguide. In this long wavelength approximation, all inhomogeneous terms and all coefficients in the linear system of equations for all Y_i in (2.58) are fully explicit. Then, the solution of the multiple scattering of an electromagnetic wave by N parallel anisotropic cylindrical waveguides boils down to solve such an algebraic system for all Y_i. It may have some interest to have treated the above cases in which all D_{ij} are adequately larger than the other length parameters. In fact, such cases could provide some clue or some starting approximation for other situations in which D_{ij}'s be only slightly or barely larger than the transverse dimensions of the waveguides and the typical wavelengths of light.

2.10.6 Multiple Scattering by N Parallel Anisotropic Waveguides: Approximate Calculation Using Sampling Theorem

The computation of the scattered field for an array of parallel cylindrical anisotropic waveguides is not an easy task. We shall now outline the results of an approximate calculation in which the separation between two neighboring waveguides is not appreciably larger than their transverse size (R), based on the application of sampling methods.[59] The latter methods have already been employed in previous works in optical diffraction theory[60] and biological waveguides.[61]

A summary of the sampling theorem is given in Appendix F. For convenience, we shall change some notations. Thus, (x, y) and $1/(2B)$, employed in Appendix F, are replaced here by (x_1, x_2) and $d/2$, respectively. A point $(nd/2, md/2)$ for each (n, m) is associated to one waveguide. The distance $d/2$ gives a scale characterizing the average separation between any two adjacent waveguides (say, between two axes suitably chosen in them). Roughly speaking, the transverse size of each waveguide (say, twice its radius, R) should not exceed lengths that are about that average separation ($d/2$); this is the so-called Nyquist limit. In some cases, $2R$ may even be allowed to exceed $d/2$ slightly, but not much; in such a case, numerical studies are required in order to check the reliability of those values. Let us recall the form of the sampling theorem as given in Eq. (F.4) with the function g replaced by $h = h(\boldsymbol{x}) = h(x_1, x_2)$, which is a column vector with two components. Each of the latter are, in turn, supposed to be band-limited functions (see Appendix F). One has the following identity, provided by the sampling theorem:

$$h(x_1, x_2) = \sum_{n=-\infty}^{+\infty} \sum_{m=-\infty}^{+\infty} h\left(\frac{nd}{2}, \frac{md}{2}\right) \frac{\pi}{4} \times \frac{2J_1(2\pi((x_1 - nd/2)^2 + (x_2 - md/2)^2)^{1/2}/d)}{2\pi((x_1 - nd/2)^2 + (x_2 - md/2)^2)^{1/2}/d} \tag{2.63}$$

$J_1(x)$ is the ordinary Bessel's function of order 1.[56]

In particular, Eq. (2.63) becomes an identity if $h(\boldsymbol{x})$ and $h(\frac{nd}{2}, \frac{md}{2})$ are replaced by $h^{(0)}(\boldsymbol{x}) = h^{(0)}(x_1, x_2)$ and $h^{(0)}(\frac{nd}{2}, \frac{md}{2})$, respectively.

Next, we perform the following approximation on Eq. (2.63): we replace the double infinite series in it by two finite sums, so that the total number of terms in the latter coincides with the total number of parallel cylindrical anisotropic waveguides. Then, the identity (2.63) becomes the approximate formula:

$$h(x_1, x_2) \simeq \sum_{n,m} h\left(\frac{nd}{2}, \frac{md}{2}\right) \frac{\pi}{4} \times \frac{2J_1((2\pi/d)((x_1 - nd/2)^2 + (x_2 - md/2)^2)^{1/2})}{(2\pi/d)((x_1 - nd/2)^2 + (x_2 - md/2)^2)^{1/2}} \tag{2.64}$$

After that approximation, notice the following. Let $h(\boldsymbol{x})$ and $h(\frac{nd}{2}, \frac{md}{2})$ be replaced by $h^{(0)}(\boldsymbol{x}) = h^{(0)}(x_1, x_2)$ and $h^{(0)}(\frac{nd}{2}, \frac{md}{2})$, respectively, in Eq. (2.64). Then, one no longer has an identity, that is, the left-hand side of Eq. (2.64) and its right-hand side are not equal to each other. Clearly, their discrepancy becomes the smaller; the larger is the total number of terms in the two finite sums in Eq. (2.64). Of course, these remarks (the discrepancy and its reduction, as the total number of terms retained increases) also apply if, in the application of Eq. (2.64) for an array of parallel cylindrical anisotropic waveguides, both $h(x_1, x_2)$ and $h(\frac{nd}{2}, \frac{md}{2})$ stand for the total magnetic field (that given by Eq. (2.53)). However, the latter application would appear to be useless. In fact, one would not know, *a priori*, the total field $(h(\frac{nd}{2}, \frac{md}{2}))$ at the finite number of points $(nd/2, md/2)$ associated to the terms retained in the two finite sums in Eq. (2.64).

Fortunately, at this stage, we can still employ Eq. (2.64) for an approximate computation of the total magnetic field (given by (2.53)), provided that we make the following additional assumption. We approximate $h(\frac{nd}{2}, \frac{md}{2})$ in the right-hand side of Eq. (2.64) by the total magnetic field corresponding to the scattering by just one waveguide, namely the one corresponding to $(x_1 = nd/2, x_2 = md/2)$. In this way, one profits from the knowledge of the total field corresponding to the scattering by single waveguides which is simpler to obtain. In other words, such a $h(\frac{nd}{2}, \frac{md}{2})$ is approximated by the solution of Eq. (2.49) for the single waveguide corresponding to $(nd/2, md/2)$. Equivalently, which may add a bit more insight, $h(\frac{nd}{2}, \frac{md}{2})$ is replaced by the right-hand side of (2.53), when, in the latter, we approximate the full $h^{(0)} + \sum_{i=1}^{N}(H_0^{(1)}/4i)\tau_{w,i}h_i$ just by $h^{(0)} + (H_0^{(1)}/4i)\tau_{w,i}h^{(0)}$, the retained i corresponding to $(nd/2, md/2)$. In turn, $h^{(0)} + (H_0^{(1)}/4i)\tau_{w,i}h^{(0)}$ is approximated by the right-hand side of Eq. (2.41), with the adequate $j^{(1)}(\boldsymbol{x}')$ (obtained upon replacing $h(\boldsymbol{x}')$ by $h^{(0)}(\boldsymbol{x}')$ in $j(\boldsymbol{x}')$). That is, $h^{(0)} + (H_0^{(1)}/4i)\tau_{w,i}h^{(0)}$ is approximated by the Debye-Born-Rayleigh-Gans approximation. Of course, if there were no scattering ($\tau_{w,i} = 0$ for all i, say, for all $(nd/2, md/2)$), then the resulting (2.64) would reduce to the approximate form of the sampling theorem corresponding to $h^{(0)}(x_1, x_2)$ discussed above.

The spirit of the above approximations is that the resulting (2.64) could still yield an acceptable approximation for the total magnetic field when multiple scattering effects are included, that is, that provided by the multiple scattering approach. Alternatively, one expects that (2.64) would provide a reasonable approximation for (2.53).

Depending on the symmetry of the problem, different sampling lattices may be used. Eqs. (2.63) and (2.64) correspond to one of such choices. See Figure 2.5.

Applications of (2.64) for transverse sizes of the waveguides and average separations between adjacent ones about the micron range have been carried out.[20,31] In the numerical calculations carried out in the latter references, the values $d = 2\,\mu m$ and $R = 0.75\ \mu m$ have been employed. Therefore, $2R = 1.5\ \mu m$ is, *a priori*, slightly beyond the $2R \leq d/2$ bound (Nyquist limit). However, no artifacts have been observed upon performing the numerical computations, so that the results of the different analysis[20,31] appear to be reasonable.

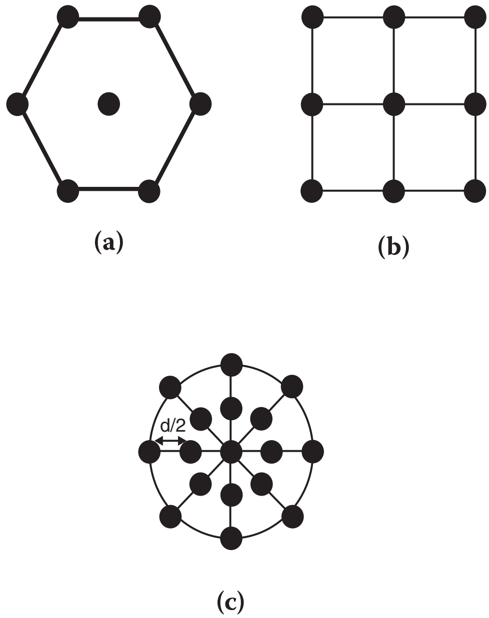

FIGURE 2.5 Three different geometries of the sampling lattice. Eqs. (2.63), (2.64) and (F.4) correspond to c), while Eq. (F.2) corresponds to b).

2.11 ANISOTROPIC DIELECTRIC WAVEGUIDES WITH PHOTO-ELASTIC EFFECT

We continue to assume that the non-vanishing ϵ_{ij} are real for typical frequencies of light, at least, approximately (absence of absorption).

2.11.1 Scattering

Let us consider an extended isotropic and homogeneous reference medium, with real constant dielectric permittivity ϵ_0. Let N ($\geq$ 1) parallel cylindrical dielectric waveguides be located inside that medium. The latter are supposed to be isotropic (and optically isotropic) to some zeroth-order (or leading order) approximation or in the absence of externally applied forces or actions. Those waveguides have dielectric permittivity tensor $\epsilon_{ik} = \epsilon_e \delta_{ik}$, $i, k = 1, 2, 3$, relative to that of the surrounding medium. In a next-to-leading order approximation or under externally applied forces, small additional internal stresses σ_{ik} inside those waveguides should be taken into account, so that the latter become optically anisotropic by virtue of the photo-elastic effect (as explained in Section 2.5). Then, the induced relative dielectric permittivity tensor ϵ_{ik} of the waveguides is given by Eq. (2.10).

In a strict sense, when the photo-elastic effect is taken into account, ϵ_{ik} as given by Eq. (2.10) lies outside the domain of validity of the simplifications considered in Subsection 2.10.1, which enabled reduction of the three-dimensional problem to a two-dimensional one. In fact, one may expect that, by virtue of the photo-elastic effect, one has $\epsilon_{13} \neq 0$ and $\epsilon_{23} \neq 0$, in general and, so, the simpler (two-dimensional) scattering theory of Section 2.10 would not apply. Instead, the more general (three-dimensional) one as outlined in Section 2.8 should be employed, but its use involves a larger amount of computational work. In order to avoid three-dimensional complications wherever possible, we shall suppose, at least tentatively, that ϵ_{13} and ϵ_{23} can still be regarded as negligible, say, at the present next-to-leading order approximation. With this simplifying assumption, strained cylindrical parallel waveguides, in which the induced anisotropy comes from the photo-elastic effect, can still be treated through the simpler two-dimensional procedures cited in Section 2.10, as we shall now outline. We shall summarize the analysis carried out,[20,31] in which further simplifying assumptions were also made. Suitable components of the stresses σ_{ik} were taken as proportional to the transverse force per unit length applied to each waveguide. Thus, for a force (with absolute magnitude F) applied parallel to the x_2 axis, the mechanical effects will be produced in the (x_1, x_2) plane. Then, σ_{11} is estimated to be $F/(\pi R^2)$, and $\sigma_{22} = -3\sigma_{11}, \sigma_{33} = 0$ with all the remaining $\sigma_{ik} \simeq 0, i \neq k$. See Figure 2.6. With the induced anisotropy due to the photo-elastic effect, $\epsilon_{12} = \epsilon_{21} \simeq 0$ were regarded also as negligible. Then, the non-vanishing elements of ϵ_{ik} are:

$$\begin{aligned}
\epsilon_{11} &\simeq \epsilon_e + a_1\sigma_{11} + a_2\sigma_{22} + a_2\sigma_{33} \\
\epsilon_{22} &\simeq \epsilon_e + a_2\sigma_{11} + a_1\sigma_{22} + a_2\sigma_{33} \\
\epsilon_{33} &\simeq \epsilon_e + a_1\sigma_{11} + a_2\sigma_{22} + a_1\sigma_{33}
\end{aligned} \tag{2.65}$$

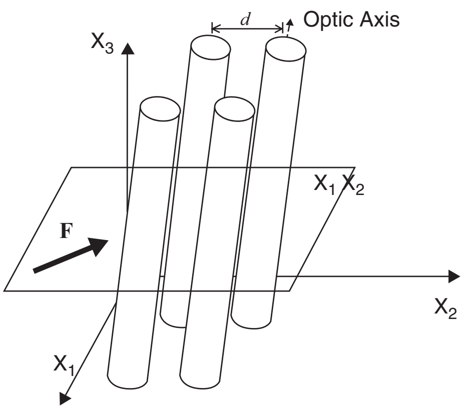

FIGURE 2.6 Model for the photo-elastic effect. A weak external force is applied in the $(x_1,$ $x_2)$ plane. The optic axis of each waveguide, when the external force is applied, is displayed (the optic axis of each waveguide is parallel to the x_3 axis, in the absence of external force). The angle between the optic axis of each waveguide (when the external force is applied) and the x_3 axis is assumed to be small.

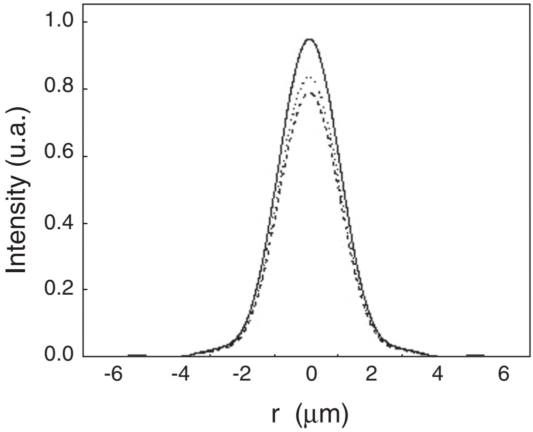

FIGURE 2.7 Spatial dependence of the forward-scattering light intensity in an interval about the forward direction (a.u.= arbitrary units). Dotted curve: zero applied force ($F = 0$). Dashed curve: $F = 0.01$ *Newton*, light polarized along x_1. Solid curve: $F = 0.01$ *Newton*, light polarized light along x_2. The external force F is applied along the x_2 direction.

a_1 and a_2 being the elastic-optical constants. Then, under the action of the externally applied force, each waveguide behaves as a uniaxial crystal. At this stage, the analysis of the total field for one single waveguide (Subsections 2.10.3 and 2.10.5) and for N parallel waveguides (using the approximations in Subsection 2.10.6 and the sampling theorem) can be directly employed. This has led to detailed numerical computations.[20,31]

The results of those computations for the intensity of light scattered in an interval about the forward direction are displayed in Figure 2.7. This figure shows the intensities for scattered light without external force ($F = 0$) and with a given value of the applied force ($F \neq 0$). In the latter case, results are also displayed for light polarized along different directions in the (x_1, x_2) plane. Figure 2.8 shows the intensity for light scattered in the forward direction against the strength of the applied force F, also for different polarizations of light in the (x_1, x_2) plane.

2.11.2 Possible Applications to Stress Sensing

The multiple scattering of light by an array of birefringent optical waveguides (arising from mechanical stresses), as described in the previous subsection, could provide another alternative for stress sensors.[31] The question of physical interest is to estimate, upon combining experimental data regarding light scattering by the strained waveguides (due to the photo-elastic effect) and theory, what the stresses σ_{ik} are; this is what stress sensing is about. One would study experimentally the scattering of

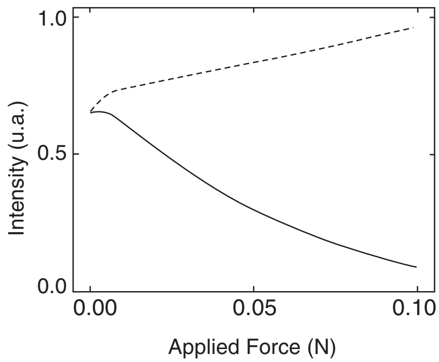

FIGURE 2.8 Forward-scattering intensity of light versus the strength F of the external force (applied along the x_2 direction) in *Newton* (N) (a.u. = arbitrary units). The solid curve corresponds to X-polarized light and the dotted curve to Y-polarized light.

light by the anisotropic waveguides (with $\sigma_{ik} \neq 0$). We suppose that we know, with adequate accuracy, ϵ_e and the elastic-optical constants a_1 and a_2 for the waveguides. One would compare the resulting experimental intensity distribution of scattered light with the one for the case in which those waveguides were isotropic (not subject to stresses, with $\sigma_{ik} = 0$). The comparison of those distributions would provide information about σ_{ik}, that is, of the state of internal stress of the waveguides and of the externally applied force (which gave rise to σ_{ik}).

Detailed numerical studies[20,31] show that the major impact of stress occurs at the central peak of the scattered light profile, that corresponds to forward scattering. This fact is what the numerical results given in Figure 2.7 display in a very neat way. When the distribution of the scattered light profile is plotted in an interval about the forward direction, it shows a central peak corresponding precisely to forward scattering. This result may be very convenient for practical purposes, since the experimental detection of light scattered in the forward direction may be performed easily in various situations. Figure 2.8 shows the forward scattering intensity for x_1- and x_2-polarized light as a function of the strength F of the externally applied force along the x_2 direction.

Even for moderate values as $F = 0.05$ *Newton*, a difference around 60 per cent between the intensities of light corresponding to both polarizations is observed. Thus, since the amount of change of the intensities for both light polarizations is directly related to the strength of the applied force, Figure 2.8 could provide a calibration curve for a stress-sensing system.[20] One main consequence of stress is the loss of symmetry due to the appearance of two privileged directions in the (x_1, x_2) plane, orthogonal to the axis of the waveguides (the x_3-axis): the axis parallel to the external force (say, the x_2-axis) and the perpendicular axis (the x_1-axis). The asymmetry induced by stress between x_1- and x_2-polarized light provides a method to assess the direction of application of the external force.[62]

2.12 CONFINED PROPAGATION OF LIGHT ALONG ANISOTROPIC WAVEGUIDES

As in Section 2.10, we shall also assume that $\epsilon_{13} = \epsilon_{23} = 0$ and that the remaining non-vanishing ϵ_{ij} are real for typical frequencies of light at least approximately (negligible absorption). When confined propagation of the classical electromagnetic wave along the anisotropic cylindrical waveguides occurs, β (also real) is named the propagation constant. For confined propagation, there are neither an incoming electromagnetic field nor physically propagating waves very far from the waveguides in the $\boldsymbol{x}$-plane.

The confined propagation along the anisotropic cylindrical waveguides is described by a set of propagation modes $h(\boldsymbol{x})_\alpha$. α denotes a suitable set of labels, so that one choice of values for those labels characterizes and distinguishes one propagation mode. Each $h(\boldsymbol{x})_\alpha$ fulfills the homogeneous version of Eq. (2.38) corresponding to $h^{(0)}(\boldsymbol{x}) \equiv 0$ (absence of propagating waves very far from the waveguides) and pure imaginary K ($K^2 < 0$). Then:

$$h(\boldsymbol{x})_\alpha = \int d^2\boldsymbol{x}' \frac{H_0^{(1)}(K \mid \boldsymbol{x} - \boldsymbol{x}' \mid)}{4i} j(\boldsymbol{x}')_\alpha \tag{2.66}$$

where $j(\boldsymbol{x}')_\alpha$ is given by the right-hand side of Eqs. (2.34) and (2.35), with $h(\boldsymbol{x})$ replaced by $h(\boldsymbol{x})_\alpha$. The integration is extended over the whole cross-sections of all waveguides. In the case of $N > 1$, one can interpret physically the confined propagation by stating that an exchange of energy of the electromagnetic field among the N waveguides occurs. There is, then, an effective coupling among those waveguides ("cross-talk").

2.12.1 One Cylindrical Waveguide

Equation (2.66) describes the confined propagation along one anisotropic cylindrical waveguide. The integration in (2.66) is now performed over the cross-sections of that unique waveguide. Let us suppose that all ϵ_{ii} are slightly larger than unity and that ϵ_{12} is small. Let us also assume that K (pure imaginary) is small in the sense that the dimensionless product $\mid K \mid R$ is smaller than unity. Physically, this will amount to restricting the analysis to the case where the anisotropic cylindrical waveguide can support only one pair of non-degenerate propagation modes, eventually those of lowest order (in the long wavelength and weakly guiding approximations). With the understanding that such a pair is regarded as one propagation mode which, in turn, could exist with two different values for K, we regard and denote such an anisotropic waveguide as a monomode. Such a mode is the fundamental one and it is non-degenerate. Then, for such values of K, one can employ the approximation (D.5) in the second term of the right-hand side of Eq. (2.66). For consistency, we neglect the $\boldsymbol{x}'$ dependence in $h(\boldsymbol{x})_\alpha$ both inside and outside the integral, so that $h(\boldsymbol{x})_\alpha \simeq h_\alpha$, with constant components $H_1\alpha$ and $H_2\alpha$. Hence:

$$h_\alpha \simeq \frac{1}{2\pi} \ln[-2^{-1} i K R \exp\gamma] \int d^2\boldsymbol{x}' j(\boldsymbol{x}')_\alpha \tag{2.67}$$

Notice that ϵ_{ij} may still depend (smoothly) on $\boldsymbol{x}'$. Then, due to the latter, there could still be some $\boldsymbol{x}'$-dependence in $j(\boldsymbol{x}')_\alpha$, which now has, approximately, the following components:

$$(j(\boldsymbol{x}')_\alpha)_1 = -(\omega/v)^2(\epsilon_{22} - 1)H_{1\alpha} + (\omega/v)^2\epsilon_{21}H_{2\alpha} \tag{2.68}$$

$$(j(\boldsymbol{x}')_\alpha)_2 = -(\omega/v)^2(\epsilon_{11} - 1)H_{2\alpha} + (\omega/v)^2\epsilon_{12}H_{1\alpha} \tag{2.69}$$

Compare the approximate Eqs. (2.68) and (2.69) with the exact Eqs. (2.34) and (2.35). Eq. (2.67) with Eqs. (2.68) and (2.69) constitutes a linear homogeneous system of two equations for the two constant magnetic field components $H_{1\alpha}$ and $H_{2\alpha}$ of h_α. The necessary and sufficient condition for the existence of a non-trivial solution of that system (namely, that $H_{1\alpha}$ and $H_{2\alpha}$ do not vanish identically) is that the determinant of the 2×2 matrix for that system vanishes. Physically, the vanishing of that determinant yields the dispersion relation for the propagation modes of the monomode anisotropic waveguide. Recall that $K^2 = (\omega/v)^2 - \beta^2$ and that K is pure imaginary, so that we write $K = iK_\pm$, where both K_+ and K_- are real. Through some algebra, Eq. (2.67) with Eqs. (2.68) and (2.69) yields:

$$\ln[2^{-1}K_\pm R \exp\gamma] \simeq -\pi\frac{[N_1 - (\pm)N_2]}{D} \tag{2.70}$$

$$N_1 = \int d^2\boldsymbol{x}(\epsilon_{11} + \epsilon_{22} - 2) \tag{2.71}$$

$$N_2 = \left[\left(\int d^2\boldsymbol{x}(\epsilon_{11} - \epsilon_{22})\right)^2 + 4\left(\int d^2\boldsymbol{x}\epsilon_{12}\right)^2\right]^{1/2} \tag{2.72}$$

$$D = (\omega/c)^2\left[\left(\int d^2\boldsymbol{x}(\epsilon_{11} - 1)\right)\left(\int d^2\boldsymbol{x}(\epsilon_{22} - 1)\right) - \left(\int d^2\boldsymbol{x}\epsilon_{12}\right)^2\right] \tag{2.73}$$

which confirm that the anisotropic waveguide under the long wavelength and weakly guiding approximations, does support only one pair of non-degenerate propagation modes.

If the waveguide is optically isotropic, then $\epsilon_{11} = \epsilon_{22}$ and $\epsilon_{12} = 0$, so that $N_2 = 0$ and $K_+ = K_-$ (degeneracy). Birefringence disappears and Eq. (2.70) becomes an approximate dispersion relation for a monomode isotropic waveguide, also in the long wavelength and weakly guiding approximations. This agrees with the properties of the degenerate fundamental (or lowest order) mode of a monomode isotropic waveguide outlined in Section 2.6.

The existence of two solutions K_+ and K_- is the actual counterpart of the fact that the Fresnel equation had two solutions (recall Subsection 2.2.2).

The book by Snyder and Love[10] summarizes some detailed studies about the confined propagation of light in one homogeneous planar waveguide with step profile for the relative dielectric permittivity tensor. As the components of the latter are constant, except for finite discontinuities at the surfaces of the waveguide, the planar geometry allows for the partial differential equations to be separable in Cartesian coordinates and to be exactly solvable. Those authors[10] also discussed, quite succinctly, some aspects of the approximate analysis for one anisotropic waveguide with other geometries in the weakly guiding approximation. Our analysis in this subsection, based upon a previous work,[19] provides a non-trivial generalization of their studies.[10]

2.12.2 N Parallel Cylindrical Waveguides: Approximations

We again consider the case with all (N) parallel anisotropic waveguides and we now treat the confined propagation of electromagnetic radiation along those N waveguides (so that K is also pure imaginary).[63] We shall concentrate in modifying succinctly the multiple scattering approach for N parallel anisotropic waveguides discussed in Subsection 2.10.5. The total magnetic field is $h_\alpha(\boldsymbol{x})$. The basic modification consists in setting $h^{(0)}(\boldsymbol{x}) \equiv 0$ in the exact Eqs. (2.53) and (2.54) (as there are neither incoming electromagnetic field nor physically propagating waves very far from any of the parallel anisotropic waveguides), h and h_i being replaced by h_α and $h_{\alpha,i}$, respectively. Then:

$$h_\alpha = \sum_{i=1}^{N} \frac{H_0^{(1)}}{4i} \tau_{w,i} h_{\alpha,i} \tag{2.74}$$

$$h_{\alpha,i} = \sum_{j=1, j\neq i}^{N} \frac{H_0^{(1)}}{4i} \tau_{w,j} h_{\alpha,j} \tag{2.75}$$

Eq. (2.75) now becomes a homogeneous system of linear equations for all $h_{\alpha,i}$, $i = 1, \ldots, N$.

Let all separations among waveguides be adequately larger than their transverse dimensions (R). Then, one has new constant column vectors $Y_{\alpha,i}(\boldsymbol{u}_{si})$, $s \neq i$, also given by (2.57). The latter fulfills a homogeneous linear system implied by Eq. (2.75) and similar to (2.58), with two crucial modifications: K is pure imaginary and, of course, $Y_j^{(0)}(\boldsymbol{u}_{si}) \equiv 0$. Each $\Lambda_{ij}(\boldsymbol{u}_{si}, \boldsymbol{u}_{ij})$ continues to be given by (2.60), also with pure imaginary K. The homogeneous linear and purely algebraic system for all $Y_i(\boldsymbol{u}_{si})$, $s \neq i$, reads:

$$Y_i(\boldsymbol{u}_{si}) = \sum_{j=1, j\neq i}^{N} \Lambda_{i,j}(\boldsymbol{u}_{si}, \boldsymbol{u}_{ij}) Y_j(\boldsymbol{u}_{ij}) \tag{2.76}$$

Moreover, let us suppose that $D_{ij} > 2\pi / \mid K \mid > R$, that is, each waveguide is monomode and the separation between any pair of waveguides is larger than the transverse effective width of each individual propagation mode ($2\pi / \mid K \mid$). Then, $\Lambda_{ij}(\boldsymbol{u}_{si}, \boldsymbol{u}_{ij})$ is given by (2.62), with pure imaginary K. In turn, the double integral $\int d^2\boldsymbol{x}' \int d^2\boldsymbol{x}'' \tau_{w,i}$ is given approximately by (2.52), also with pure imaginary K. In this case, the homogeneous system for $Y_{\alpha,i}(\boldsymbol{u}_{si})$ can be solved explicitly. Its solution gives the dispersion relation for the propagation modes of the N-coupled monomode anisotropic waveguides (say, the counterpart of (2.70) which includes "cross-talk"). Some numerical estimates and applications for $N = 2$ have also been carried out.[63]

2.13 CONCLUSION AND FINAL COMMENTS

We have summarized two closely interrelated subjects: a) several physically relevant cases in which optical anisotropy occurs, and b) some general features of classical electromagnetic wave scattering by and confined propagation along optically anisotropic materials. Detailed applications of b) to all systems included in a) lie outside our scope here, but we tried to emphasize their relevance and reciprocal relationship and we have concentrated on certain applications. More specifically:

1. We have summarized a rather general formulation of the scattering (and multiple scattering) of a classical electromagnetic wave by N optically anisotropic objects of arbitrary shapes, relative orientations and separations. The interest in presenting this formalism lies in its generality and flexibility. It includes scattering by optically isotropic objects (in which the dielectric permittivity tensor reduces to a scalar). As a particular but important case, it also provides the basis for analyzing the scattering by parallel cylindrical optically anisotropic waveguides. It could also provide a starting point for studying more general configurations, for instance, the inclusion of misalignments of cylindrical waveguides.
2. We have concentrated on the electromagnetic scattering by $N(\geq 1)$ parallel cylindrical optically anisotropic dielectric waveguides including long wavelength approximations and the case in which the anisotropy is due to stress birefringence.
3. We have summarized recent research about the effect of external stress on scattering by an array of parallel cylindrical waveguides (with anisotropies due to the photo-elastic effect). By analyzing the light scattered (specifically in the forward direction) by dielectric fibers that were optically isotropic first and at a later stage became optically anisotropic due to stress, physically relevant information can be obtained about the externally applied force giving rise to the photo-elastic effect. That could be the basis of another kind of optical stress sensor.
4. We have treated the confined propagation along cylindrical anisotropic dielectric waveguides; in particular, the long wavelength approximation for one waveguide (monomode confined propagation) has been analyzed.

The dominant effects in the biological waveguides in the eye (those in the retinal nerve fiber layer and in the retinal photoreceptors) seem to correspond to optical isotropy, at least under normal functioning conditions. Optical anisotropies in those waveguides may arise under pathological functioning conditions (say, due to the abnormal stresses giving rise to the photo-elastic effect). Then, (weak) scattering by anisotropic waveguides could play a role. In this connection, we mention some experimental results on the Stiles-Crawford effect of first kind (*SCE-I*).[50] Such results seem to describe changes appearing in the retinal nerve fiber layer as it is exposed to some tractions and external mechanical stresses. The latter have motivated further modeling and approximate numerical estimates for the retinal nerve fiber layer, regarded as a bundle of biological waveguides in which the photo-elastic effect is included.[64] In the latter work, the intensity distribution of the light scattered by the array of waveguides is connected with the *SCE-I*, since it would reflect the waveguiding properties of the retina and it would be a psychophysical consequence of the directional sensitivity of the retinal photoreceptors.

One open important question is whether optical fibers of the nerve disk require any specific birefringence properties along with the photo-elastic effect (and dichroism) or, opposite to it, the behavior they exhibit (in relation to the optical mechanism for waveguiding and scattering of the incoming luminous radiation) is due to accumulative stress forces acting permanently throughout the whole life of each individual (infancy and adult stages would not exhibit the same photo-elastic properties).

ACKNOWLEDGMENTS

M. L. Calvo wishes to acknowledge the support of Ministerio de Ciencia y Tecnología (Project TEC2005-02186) of Spain. We are also grateful to Dr. G. F. Calvo for having provided valuable help with the LaTex files. The kind help provided by Profs. A. Munoz Sudupe and L. A. Fernandez regarding the figures is also acknowledged.

Appendix A

Fresnel Equation, Birefringence and Polarization Vectors

We consider Eqs. (2.3) for an extended homogeneous anisotropic dielectric medium and the propagation in it of an electromagnetic plane wave with frequency ω and wavevector $\bar{k} = (k_1, k_2, k_3)$. That wave is described by $\mathbf{H}' = \mathbf{H}'_0 \exp i\bar{k}\bar{x}$, $\mathbf{H}'_0$ being constant. Moreover, we shall impose that $\mathbf{H}'_0$ fulfills $\bar{k}\mathbf{H}'_0 = 0$, so that the second relation in (2.3) be automatically fulfilled. Then, the first relation in (2.3) becomes:

$$\mathbf{H}''_0 + (\omega/v)^2 \mathbf{H}'_0 = 0 \tag{A.1}$$

$$\mathbf{H}''_0 = \bar{k} \times [(\tilde{\epsilon})^{-1} \bar{k} \times \mathbf{H}'_0] \tag{A.2}$$

$\times$ denoting vector product. Eq. (A.1) is also consistent with the second relation in (2.3). Let σ be an index which takes on only two values (say, σ_1 and σ_2). Also, let $\bar{\epsilon}(\bar{k}, \sigma)$ be two real or complex three-dimensional (column) vectors fulfilling $\bar{k}\bar{\epsilon}(\bar{k}, \sigma) = 0$ for $\sigma = \sigma_1, \sigma_2$, as well as $\bar{\epsilon}(\bar{k}, \sigma)^+ \bar{\epsilon}(\bar{k}, \sigma') = \delta_{\sigma,\sigma'}$ and $\sum_\sigma (\bar{\epsilon}(\bar{k}, \sigma))_i (\bar{\epsilon}(\bar{k}, \sigma)^+)_j = \delta_{i,j} - (k_i k_j / \bar{k}^2)$, $i, j = 1, 2, 3$. $\delta_{i,j}$ denotes here the Kronecker delta symbol, namely, $\delta_{i,i} = 1$ and $\delta_{i,j} = 0$ for $i \neq j$. The superscript $+$ denotes adjoint (that is, complex conjugate and matrix transposition), so that $\bar{\epsilon}(\bar{k}, \sigma)^+$ is a row vector. The $\bar{\epsilon}(\bar{k}, \sigma)$'s are nothing but the standard linear (real) or circular (complex) unit polarization vectors.[51] They are given by the same expressions as for electromagnetic wave propagation in vacuum.

It follows that $\mathbf{H}'_0 = \sum_\sigma (\mathbf{H}'_0)_\sigma \bar{\epsilon}(\bar{k}, \sigma)$, $\mathbf{H}''_0 = \sum_\sigma (\mathbf{H}''_0)_\sigma \bar{\epsilon}(\bar{k}, \sigma)$, where $(\mathbf{H}'_0)_\sigma$ and $(\mathbf{H}''_0)_\sigma$ are, respectively, the two components of $\mathbf{H}'_0$ and $\mathbf{H}''_0$ with respect to the basis formed by the two vectors $\bar{\epsilon}(\bar{k}, \sigma)$. Eq. (A.2) implies necessarily $(\mathbf{H}''_0)_\sigma = \sum_{\sigma'} (\tilde{\Lambda}_2)_{\sigma,\sigma'} (\mathbf{H}'_0)_{\sigma'}$. The elements $(\tilde{\Lambda}_2)_{\sigma,\sigma'}$ of the 2×2 matrix $\tilde{\Lambda}_2$ (which depend quadratically on $\bar{k}$, bilinearly on $\bar{\epsilon}(\bar{k}, \sigma)$ and $\bar{\epsilon}(\bar{k}, \sigma)^+$ and linearly on $((\tilde{\epsilon})^{-1})_{ii})$ are somewhat lengthy. Neither will they be given here nor will their explicit expressions be necessary for the conclusion that follows. The latter equation for $(\mathbf{H}''_0)_\sigma$ and Eq. (A.1) yield:

$$\sum_{\sigma'} (\tilde{\Lambda}_2)_{\sigma,\sigma'} (\mathbf{H}'_0)_{\sigma'} + (\omega/v)^2 (\mathbf{H}'_0)_{\sigma'} = 0 \tag{A.3}$$

Eq. (A.3) is a linear homogeneous system of two equations for the two amplitudes $(\mathbf{H}_0')_{\sigma'}$. The compatibility condition for that system to have a nonzero solution for those $(\mathbf{H}_0')_{\sigma'}$ (namely the vanishing of the determinant) is a quadratic equation in ω^2, for given $\bar{k}$. The latter property, then, follows from the physical fact that only two independent states of polarization are possible for an electromagnetic plane wave. That compatibility condition is nothing but the Fresnel equation.

Appendix B

Three-Dimensional Transverse Green's Function

We write $G_{Tr}(\bar{x}) = (G_{Tr}(\bar{x})_{l,l'})$, $l, l' = 1, 2, 3$ where $G_{Tr}(\bar{x})_{l,l'}$ is the (l, l')-th component of the transverse tensor Green's function $G_{Tr}(\bar{x})$. By definition, $G_{Tr}(\bar{x})$ is constructed so that for any $\bar{x}$ in three-dimensional space:

$$\left[\Delta + K_{cl}^2\right] G_{Tr}(\bar{x})_{l,l'} = \delta_{Tr}^{(3)}(\bar{x})_{l,l'}, \quad \sum_{l=1^3} \frac{\partial G_{Tr}(\bar{x})_{l,l'}}{\partial x_l} = 0 \tag{B.1}$$

$\delta_{Tr}^{(3)}(\bar{x})_{l,l'}$ stands for the (l, l')-th component of the three-dimensional transverse Dirac delta function. It is given by:

$$\delta_{Tr}^{(3)}(\bar{x})_{l,l'} = \frac{1}{(2\pi)^3} \int d^3\bar{q} \left[\delta_{l,l'} - \frac{q_l q_{l'}}{\bar{q}^2}\right] \exp i\bar{q}\bar{x} \tag{B.2}$$

In turn, $\delta_{l,l'}$ is the Kronecker delta symbol and $\bar{q} = (q_1, q_2, q_3)$. One finds:[53]

$$G_{Tr}(\bar{x})_{l,l'} = \frac{1}{(2\pi)^3 K_{cl}^2} \int d^3\bar{q} \left[\frac{q_l q_{l'} - K_{cl}^2 \delta_{l,l'}}{\bar{q}^2 - (K_{cl}^2 + i\eta)} - \frac{q_l q_{l'}}{\bar{q}^2}\right] \exp i\bar{q}\bar{x} \tag{B.3}$$

where it is assumed that the limit $\eta \to 0$, with $\eta > 0$, is taken after having carried out the integration over $\bar{q}$.

Upon performing the integration over $\bar{q}$ (in particular, the one over $\mid \bar{q} \mid$ by means of Cauchy's residue theorem), one arrives at the explicit expression for $G_{Tr}(\bar{x})_{l,l'}$:

$$G_{Tr}(\bar{x})_{l,l'} = -\frac{\exp iK_{cl} \mid \bar{x} \mid}{4\pi \mid \bar{x} \mid}\delta_{l,l'} + \frac{1}{4\pi K_{cl}^2} \frac{\partial^2}{\partial x_l \partial x_{l'}} \left[\frac{1 - \exp iK_{cl} \mid \bar{x} \mid}{\mid \bar{x} \mid}\right] \tag{B.4}$$

Two interesting properties of $G_{Tr}(\bar{x})_{l,l'}$ are its short and long distance behaviors. For $\mid \bar{x} \mid \to 0$

$$G_{Tr}(\bar{x})_{l,l'} \simeq -\frac{1}{8\pi \mid \bar{x} \mid} \left[\delta_{l,l'} + \frac{x_l x_{l'}}{\mid \bar{x} \mid^2}\right] \tag{B.5}$$

For fixed $\bar{x}'$ and $|\bar{x}| \to +\infty$, along a fixed direction (say, fixed $x_l/|\bar{x}|, l = 1, 2, 3$):

$$G_{Tr}(\bar{x} - \bar{x}')_{l,l'} \simeq -\frac{1}{4\pi \mid \bar{x} \mid}\left[\delta_{l,l'} - \frac{x_l x_{l'}}{\mid \bar{x} \mid^2}\right] \cdot \exp iK_{cl} \mid \bar{x} \mid . \exp[-iK_{cl}(\bar{x}\bar{x}')/\mid \bar{x} \mid] \tag{B.6}$$

We introduce the outgoing wavevector $\bar{k}' \equiv K_{cl}(\bar{x}/\mid \bar{x} \mid)$ and, in terms of it, we recall the two standard (real or complex) three-dimensional polarization vectors $\bar{\epsilon}(\bar{k}', \sigma)$ discussed in Appendix A. Then, the long-distance Eq. (B.6) can be recast as:

$$G_{Tr}(\bar{x} - \bar{x}')_{l,l'} \simeq -\frac{1}{4\pi \mid \bar{x} \mid}\sum_{\sigma}(\bar{\epsilon}(\bar{k}', \sigma))_l(\bar{\epsilon}(\bar{k}', \sigma)^+)_{l'} \cdot \exp iK_{cl} \mid \bar{x} \mid . \exp[-i\bar{k}'\bar{x}'] \tag{B.7}$$

Appendix C

Alternative Two-Dimensional Formulations

We shall discuss equivalent alternatives for the two-dimensional Maxwell's equations (2.33), (2.34) and (2.35), for anisotropic cylindrical waveguides. One can also start from the system of four coupled equations for the three components H_1', H_2', H_3' in Eqs. (2.16) and (2.17), under the simplifying assumptions embodied in $\tilde{\epsilon}$, as formulated in Subsection 2.10.1. The subsystem for the first two components of the first Eq. (2.16) reads:

$$[\Delta + K_{cl}^2]H_i' = j_i', i = 1, 2 \tag{C.1}$$

$$\begin{aligned} j_1' = {} & \frac{\partial}{\partial x_2}\left[\left(\frac{1}{\epsilon_{33}} - 1\right)\left(\frac{\partial H_2'}{\partial x_1} - \frac{\partial H_1'}{\partial x_2}\right)\right] - \frac{\partial}{\partial x_3}\left[-\frac{\epsilon_{21}}{det\tilde{\epsilon}_2}\left(\frac{\partial H_3'}{\partial x_2} - \frac{\partial H_2'}{\partial x_3}\right)\right. \\ & \left. + \left(\frac{\epsilon_{11}}{det\tilde{\epsilon}_2} - 1\right)\left(\frac{\partial H_1'}{\partial x_3} - \frac{\partial H_3'}{\partial x_1}\right)\right] \end{aligned} \tag{C.2}$$

$$\begin{aligned} j_2' = {} & \frac{\partial}{\partial x_3}\left[\left(\frac{\epsilon_{22}}{det\tilde{\epsilon}_2} - 1\right)\left(\frac{\partial H_3'}{\partial x_2} - \frac{\partial H_2'}{\partial x_3}\right) - \frac{\epsilon_{12}}{det\tilde{\epsilon}_2}\left(\frac{\partial H_1'}{\partial x_3} - \frac{\partial H_3'}{\partial x_1}\right)\right] \\ & - \frac{\partial}{\partial x_1}\left[\left(\frac{1}{\epsilon_{33}} - 1\right)\left(\frac{\partial H_2'}{\partial x_1} - \frac{\partial H_1'}{\partial x_2}\right)\right] \end{aligned} \tag{C.3}$$

for any $\boldsymbol{x}$. j_1' and j_1' are the first two components of $\mathbf{j}'$. Notice that Eq. (2.30) has not been used so that H_3' has not been eliminated. One has $det\tilde{\epsilon}_2 = \epsilon_{11}\epsilon_{22} - \epsilon_{12}^2$ (which is a reminder of the fact that one is dealing with $(\tilde{\epsilon}^{-1})$.

Next, one employs the second equation in (2.3) together with (2.30) in order to express H_3 in terms of H_1, H_2. One plugs the resulting H_3 into Eqs. (C.1), (C.2) and (C.3). Then, Eqs. (C.1), (C.2) and (C.3) become a system of two equations depending only on H_1, H_2, in which $det\tilde{\epsilon}_2$ (which comes from $(\tilde{\epsilon}^{-1})$ does appear explicitly. Consequently, such a new system for H_1, H_2 does not seem to coincide in an explicitly obvious way with Eqs. (2.33), (2.34) and (2.35). The solution to the apparent paradox comes from Eq. (2.1). Thus, using the assumptions on $\tilde{\epsilon}$ and (2.29), one expresses E_1, E_2, E_3 in terms of H_1, H_2. Consequently, $\nabla \cdot (\tilde{\epsilon}\mathbf{E}') = 0$ becomes a relationship among components of $\tilde{\epsilon}$, H_1, H_2 and spatial derivatives of them. Such a constraint equation indicates that various, apparently different, systems for H_1, H_2 have to be related (not to say equivalent) to one another. The system for H_1, H_2 arising from Eqs. (C.1), (C.2) and (C.3), as derived in this appendix, and Eqs. (2.33), (2.34) and (2.35) are certainly and strictly equivalent to each other, as they both come from Maxwell's equations. We have indeed checked that fact, under the assumption that the elements of $\tilde{\epsilon} - I_3$, K^2, derivatives of the elements of $\tilde{\epsilon}$ and derivatives of H_1, H_2 are small. Then, Eqs. (2.34) and (2.35) reduce approximately to (2.33) with:

$$j_1 \simeq -(\omega/v)^2(\epsilon_{22} - 1)H_1 + (\omega/v)^2\epsilon_{21}H_2 \equiv j_{1,app} \tag{C.4}$$

$$j_2 \simeq -(\omega/v)^2(\epsilon_{11} - 1)H_2 + (\omega/v)^2\epsilon_{12}H_1 \equiv j_{2,app} \tag{C.5}$$

which are to be combined with (2.33). It is easy to see that, under similar approximations, the system for H_1, H_2 implied by Eqs. (C.1), (C.2) and (C.3) as derived in this appendix does coincide with Eqs. (2.33), (C.4) and (C.5).

Another equivalent alternative is the following. After having used Eqs. (2.29) and (2.30) in order to factor out the x_3-dependence, one continues with $\mathbf{H} = (H_1, H_2, H_3)$, without eliminating H_3, and with Eqs. (2.16) and (2.17). Then, one transforms those x_3-independent Eqs. (2.16) and (2.17) into another inhomogeneous scattering integral equation by means of a cylindrical transverse tensor Green's function.[65] The analysis in the latter reference for an isotropic cylindrical waveguide indicates the essentials of the alternative formulation, and it can be extended to the actual case of an anisotropic cylindrical waveguide. We shall omit details.

Appendix D

Outgoing Hankel's Function of Zeroth Order and Useful Approximations for It

A very important property of $H_0^{(1)}(K \mid \boldsymbol{x}-\boldsymbol{x}' \mid)/4i$ is its large distance behavior. For fixed $\boldsymbol{x}'$ and $\mid \boldsymbol{x} \mid \rightarrow +\infty$, along a fixed direction (say, fixed $x_l/ \mid \boldsymbol{x} \mid$, $l = 1, 2$):

$$\frac{H_0^{(1)}(K|\boldsymbol{x}-\boldsymbol{x}'|)}{4i} \rightarrow \frac{1}{4i}\left[\frac{2}{\pi K|\boldsymbol{x}|}\right]^{1/2} \exp i(K|\boldsymbol{x}| - \pi/4). \exp[-iK(\boldsymbol{x}\boldsymbol{x}')/|\boldsymbol{x}|] \tag{D.1}$$

Let $\epsilon(\boldsymbol{k},\sigma)$, $\sigma = \sigma_1, \sigma_2$, be two real or complex two-dimensional vectors fulfilling $\epsilon(\boldsymbol{k},\sigma)^{+}\epsilon(\boldsymbol{k},\sigma') = \delta_{\sigma,\sigma'}$ and $\sum_\sigma (\epsilon(\boldsymbol{k},\sigma))_i(\epsilon(\boldsymbol{k},\sigma)^{+})_j = \delta_{i,j}$, $i, j = 1, 2$. The superscript $+$ also denotes adjoint. Then, with $\boldsymbol{k}' \equiv K(\boldsymbol{x}/ \mid \boldsymbol{x} \mid)$, Eq. (D.1) can be reformulated as:

$$\frac{H_0^{(1)}(K \mid \boldsymbol{x}-\boldsymbol{x}' \mid)}{4i}\delta_{i,j} \rightarrow \frac{1}{4i}\left[\frac{2}{\pi K \mid \boldsymbol{x} \mid}\right]^{1/2} \exp i(K \mid \boldsymbol{x} \mid -\pi/4)$$
$$\times \exp[-i\boldsymbol{k}'\boldsymbol{x}'] \sum_\sigma (\epsilon(\boldsymbol{k}',\sigma))_i(\epsilon(\boldsymbol{k}',\sigma)^{+})_j \tag{D.2}$$

Let K be either real (scattering) or pure imaginary (confined propagation). One has the following identity, for any $\mid \boldsymbol{x}-\boldsymbol{x}' \mid$:

$$\frac{H_0^{(1)}(K \mid \boldsymbol{x}-\boldsymbol{x}' \mid)}{4i} = \frac{1}{2\pi}\ln[-2^{-1}iK \mid \boldsymbol{x}-\boldsymbol{x}' \mid \exp\gamma] + G_1(K \mid \boldsymbol{x}-\boldsymbol{x}' \mid) \tag{D.3}$$

which defines the function $G_1(K \mid \boldsymbol{x}-\boldsymbol{x}' \mid)$, trivially. Here, γ denotes Euler's constant. Explicit forms of $G_1(K \mid \boldsymbol{x}-\boldsymbol{x}' \mid)$ can be obtained upon comparing Eq. (D.3) with various known representations for $H_0^{(1)}(K \mid \boldsymbol{x}-\boldsymbol{x}' \mid)$,[58] but they will not be needed here. For fixed $\mid \boldsymbol{x}-\boldsymbol{x}' \mid \neq 0$, let $K \rightarrow 0$. Then, in such a limit, the dominant term on the right-hand side of Eq. (D.3) is the first one:[58]

$$\frac{H_0^{(1)}(K \mid \boldsymbol{x}-\boldsymbol{x}' \mid)}{4i} \rightarrow \frac{1}{2\pi}\ln[-2^{-1}iK \mid \boldsymbol{x}-\boldsymbol{x}' \mid \exp\gamma] \tag{D.4}$$

The following remark will display the physical interest of Eq. (D.4), having in mind applications for scattering and confined propagation with long wavelength. Let the area of the transverse cross-section Ω of the anisotropic waveguide be of order R^2. Let us assume that K is small in the sense that the dimensionless product $\mid K \mid R$ is small compared to unity. Let $\boldsymbol{x}$ vary arbitrarily inside the transverse cross-section Ω of the anisotropic waveguide. Then, for such values of K and for any suitably smooth function $f(\boldsymbol{x}')$ that vanishes outside the transverse cross-section Ω:

$$\int d^2\boldsymbol{x}' \frac{H_0^{(1)}(K \mid \boldsymbol{x} - \boldsymbol{x}' \mid)}{4i} f(\boldsymbol{x}') \simeq \frac{1}{2\pi} \ln[-2^{-1} i K R \exp \gamma] \int d^2\boldsymbol{x}' f(\boldsymbol{x}') \quad \text{(D.5)}$$

Notice that $\boldsymbol{x}'$ also varies inside Ω. Then, as $\boldsymbol{x}$ also varies inside the latter, $\mid \boldsymbol{x} - \boldsymbol{x}' \mid$ is, on the average, of order R. Eq. (D.5) constitutes the physical approximation based upon Eq. (D.4).

Let us now consider two separate cylindrical waveguides (say, the i-th and the j-th ones, $i \neq j$), both of them parallel to the x_3 axis. We now consider $H_0^{(1)}(K|\boldsymbol{x}-\boldsymbol{x}'|)/4i$, for $\boldsymbol{x}$ on the i-th waveguide and $\boldsymbol{x}'$ on the j-th one. In a plane orthogonal to the x_3 axis, and with respect to an arbitrary origin located in that plane, let z_i and z_j be the two-dimensional position vectors of two suitably chosen fixed points, one inside the i-th waveguide and the other inside the j-th one. Let $D_{ij} = \mid z_i - z_j \mid$ and we suppose that D_{ij} is larger than the sum of the transverse sizes of both waveguides ($D_{ij} > R_i + R_j$). We introduce, for later convenience $\boldsymbol{u}_{ij} \equiv (z_i - z_j)/D_{ij}$. We write the above $\boldsymbol{x}$ and $\boldsymbol{x}'$ as: $\boldsymbol{x} = z_i + \boldsymbol{x} - z_i$ and $\boldsymbol{x}' = z_j + \boldsymbol{x}' - z_j$. We are interested in the large distance behavior of $H_0^{(1)}(K \mid \boldsymbol{x} - \boldsymbol{x}' \mid)/4i$ for suitably large D_{ij}, for fixed $\boldsymbol{u}_{ij}$, when $\mid \boldsymbol{x} - z_i \mid$ and $\mid \boldsymbol{x}' - z_j \mid$ are smaller than D_{ij}. A computation which generalizes directly (D.1) yields:

$$\frac{H_0^{(1)}(K \mid \boldsymbol{x} - \boldsymbol{x}' \mid)}{4i} \simeq \frac{1}{4i} \left[\frac{2}{\pi K D_{ij}} \right]^{1/2} \exp i(K D_{ij} - \pi/4) \times \exp[i K \boldsymbol{u}_{ij}((\boldsymbol{x} - z_i) - (\boldsymbol{x}' - z_j))] \quad \text{(D.6)}$$

Appendix E

Equivalent Form of Integral Equations and Generalizations for Discontinuous Permittivities

Notice that in Eq. (2.38) both $h(\boldsymbol{x}')$ and spatial derivatives thereof appear inside the integral. It is possible to recast Eq. (2.38) into an equivalent form without spatial derivations of $h(\boldsymbol{x}')$. Still with the assumption that all components of $\tilde{\epsilon}$ and their first spatial derivatives are continuous throughout all space (and also across the boundaries of all waveguides), Eq. (2.38) can be re-expressed as:

$$h(\boldsymbol{x}) = h^{(0)}(\boldsymbol{x}) + \int d^2\boldsymbol{x}' \left[\frac{H_0^{(1)}(K \mid \boldsymbol{x} - \boldsymbol{x}' \mid)}{4i} P_1(\boldsymbol{x}') + P_2(\boldsymbol{x}, \boldsymbol{x}') \right] h(\boldsymbol{x}') \quad \text{(E.1)}$$

The 2×2 matrices P_1 and P_2 have been obtained explicitly.[19] The derivation of Eq. (E.1) from Eq. (2.38) proceeds by performing in the latter two integrations by parts, successively.[19]

We now comment shortly about the generalization for discontinuous $\tilde{\epsilon}$. Thus, let the components of $\tilde{\epsilon}$ and their first spatial derivatives be continuous everywhere, except across the interfaces (Σ) separating the anisotropic cylindrical waveguides from the surrounding isotropic medium. Then, generalizations of the integral Eq. (2.38) and of (E.1) (including, in both cases, boundary terms given as integrals over Σ) have also been obtained.[19] We shall omit details of those generalizations, and we limit ourselves to remark that the relevant equations are Eqs. (3.2) and Eqs. (A.11) through (A.19) in Reference 19. We also remark that the following misprints should be corrected in the formulas given in a previous work.[19] In both Eqs. (A.13) and (A.14) of that previous work,[19] a_{t2} should be replaced by a_{t1} while a_{t1} should be substituted by $-a_{t2}$.

Appendix F
Sampling Theorem

The so-called sampling theorem provides a specific procedure for representing a class of functions with interest in information and communication theories and optics. There is a very interesting account of the sampling theorem with a view toward its applications in optics.[59] For our purposes, the summary of such an account[59] to be given below will suffice.

We consider the plane (x, y) (x and y being two independent real variables in $-\infty < x < +\infty$ and $-\infty < y < +\infty$) and real or complex functions $g = g(x, y)$ (or column vectors, formed by the latter functions). To fix the ideas, we shall continue referring to functions g in this appendix, although the basics of the sampling theorem are applied to column vectors in Subsection 2.10.6 and Section 2.11. Qualitatively, the basic sampling idea is the following. We consider a suitable discrete (finite or denumerably infinite) set of points (x_j, y_j), $j = 1, \ldots$, and the set of all the resulting values $g_j = g(x_j, y_j)$ ("the array of all sampled values or data"). We would like such an array of sampled data to provide an adequate representation of the complete function g. That is, we expect that it is possible to reconstruct with sufficient accuracy, $g(x, y)$ for any (x, y) from that array of data g_j $(j = 1, \ldots)$ by interpolation or by other means. Clearly, in order for such a "sufficient accuracy" to be possible, g and the chosen discrete set of points (x_j, y_j), $j = 1, \ldots$, have to fulfill certain restrictions. The sampling theorem given below characterizes certain suitable g's and discrete sets of points (x_j, y_j) for which such a representation is exact.

It will be crucial to introduce the Fourier transform $F[g] = G = G(f_x, f_y)$ of g:

$$F[g] = G(f_x, f_y) = \int_{-\infty}^{+\infty} dx \int_{-\infty}^{+\infty} g(x, y) \exp[-i2\pi(xf_x + yf_y)]dy \qquad \text{(F.1)}$$

f_x and f_y (the "spatial frequencies") are real. In the two-dimensional spatial frequency space, a "point" is formed by one pair (f_x, f_y). The function g is, by definition, a band-limited one, if $G(f_x, f_y)$ is non-vanishing over only a finite region of the spatial frequency space (f_x, f_y).

Let g be a band-limited function. Let B_X, B_Y denote certain fixed values of the spatial frequencies f_x, f_y, respectively. One has, for any (x, y), the following identity[59]

$$g(x, y) = \sum_{n=-\infty}^{+\infty} \sum_{m=-\infty}^{+\infty} g\left(\frac{n}{2B_X}, \frac{m}{2B_Y}\right) \sin c\left(2B_X\left(x - \frac{n}{2B_X}\right)\right) \times \sin c\left(2B_Y\left(y - \frac{m}{2B_Y}\right)\right) \tag{F.2}$$

We recall that the function $\sin c(x)$ is defined as:

$$\sin c(x) \equiv \frac{\sin(\pi x)}{\pi x} \tag{F.3}$$

In this case, the discrete set of points (x_j, y_j), $j = 1, \ldots$ referred to above is denumerably infinite, and it is formed by all $(n/2B_X, m/2B_Y)$, $n = -\infty, \ldots, +\infty$, $m = -\infty, \ldots, +\infty$. The actual array of all sampled data is now formed by all $g(n/2B_X, m/2B_Y), n = -\infty, \ldots, +\infty, m = -\infty, \ldots, +\infty$. One sees immediately that Eq. (F.2) enables us to reconstruct exactly the band-limited function g for any (x, y) in terms of the actual array of all sampled data. It can be justified[59] that the maximum spacings in that discrete set of all points (x_j, y_j), that allow for exact recovery of the original function $g(x, y)$, are $1/2B_X$ and $1/2B_Y$. The set of all products $\sin c(2B_X(x - n/2B_X)) \sin c(2B_Y(y - m/2B_Y))$ gives rise in an effective way to the interpolations necessary to yield g, for any (x, y) from all $g(n/2B_X, m/2B_Y)$'s.

Eq. (F.2) is one form of the so-called Whittaker-Shannon sampling theorem, namely, the one associated with the chosen discrete set of points (x_j, y_j). There are other forms of that sampling theorem for other choices of the discrete sets of points (x_j, y_j). We shall consider one of those alternative forms (more adequate for our purposes), namely that for band-limited functions g such that $G(f_x, f_y)$ vanishes outside a circle of radius R and centered about the origin in the spatial frequency space (f_x, f_y). One now has the following alternative form of the sampling theorem:[59]

$$g(x, y) = \sum_{n=-\infty}^{+\infty} \sum_{m=-\infty}^{+\infty} g\left(\frac{n}{2B}, \frac{m}{2B}\right) \frac{\pi}{4} \times \frac{2J_1(2\pi B((x - n/2B)^2 + (y - m/2B)^2)^{1/2})}{2\pi B((x - n/2B)^2 + (y - m/2B)^2)^{1/2}} \tag{F.4}$$

where $J_1(x)$ denotes the ordinary Bessel's function of order 1.[58]

REFERENCES

1. M. Born and E. Wolf, *Principles of Optics*, 7th Ed. (Cambridge University Press, Cambridge, 1999).
2. L. D. Landau and E. M.Lifchitz, *Electrodynamics of Continuous Media* (Pergamon Press, Oxford, 1960).
3. B. E. A. Saleh and M. C. Teich, *Fundamentals of Photonics*, Wiley Series in Pure and Applied Optics (John Wiley & Sons, New York, 1991).
4. H. C. van de Hulst, *Light Scattering by Small Particles* (Dover, New York, 1981).
5. M. Kerker, *The Scattering of Light and Other Electromagnetic Radiation*, (Academic, Orlando, Florida, 1969).
6. C. F. Bohren and D. R. Huffman, *Absorption and Scattering of Light by Small Particles* (John Wiley & Sons, New York, 1983).
7. S. K. Sharma and D. J. Somerford, Scattering of Light in the Eikonal Approximation, in *Progress in Optics*, Vol. XXXIX, E. Wolf, Ed. (Elsevier Science, Amsterdam, 1997).
8. D. Marcuse, *Light Transmission Optics* (Van Nostrand Reinhold, New York, 1972).
9. D. Marcuse, *Theory of Dielectric Optical Waveguides* (Academic Press, New York, 1974).
10. A. W. Snyder and J. D. Love, *Optical Waveguide Theory* (Chapman & Hall, London, 1983).
11. E. Snitzer, *J. Opt. Soc. Am.* **51**, 491 (1961).
12. P. J. B. Clarricoats, *Optical Fibre Waveguides: A Review* in *Progress in Optics*, Vol. XIV, E. Wolf, Ed. (Elsevier, Amsterdam, 1976).
13. M. J. Adams, *An Introduction to Optical Waveguide* (John Wiley & Sons, New York, 1981).
14. M. S. Sodha and A. Ghatak, *Inhomogeneous Optical Waveguide* (Plenum Press, London, 1977).
15. A. Ghatak and K. Thyagarajan, *Introduction to Fibre Optics* (Cambridge University Press, Cambridge, 1998).
16. J. M. Enoch and F. L. Tobey, Eds., *Vertebrate Photoreceptor Optics* (Springer-Verlag, Berlin, 1981).
17. V. Lakshminarayanan and J. M. Enoch, Biological Waveguides Optics, in *Handbook of Optics*, Volume III, 2nd Ed., M. Bass, et al., Eds. (McGraw-Hill, New York, 2001).
18. J. Sakai, S. Machida and T. Kimura, *Opt. Lett.* **6**, 496 (1981).
19. R. F. Alvarez-Estrada and M. L. Calvo, *Optica Acta* **30**, 481 (1983).
20. J. Limeres, M. L. Calvo, V. Lakshminarayanan and J. M. Enoch, *J. Opt. A: Pure. Appl. Opt.* **5**, S370 (2003).
21. F. I. Harosi, Microspectrophotometry and Optical Phenomena: Birefringence, Dichroism and Anomalous Dispersion, in *Vertebrate Photoreceptor Optics*, J. M. Enoch and F. L. Tobey, Eds. (Springer-Verlag, Berlin, 1981).
22. W. Thornburg, *J. Biophys. Biochem. Cytol.* **3**, 413 (1957).
23. R. P. Hemenger, *Appl. Optics* **28**, 4030 (1989).
24. Q. Zhou and R. W. Knighton, *Appl. Opt.* **36**, 2273 (1997).
25. D. Brewster, *Phil. Trans.* 60 (1815), 156 (1816), and *Trans. Royal Soc. Ed.* **8**, 369 (1818).
26. G. Bruhat, *Optique*, Chapter XXV (Masson & Cie., Paris, 1965).
27. E. G. Coker and L. N. G. Filon, *A Treatise on Photo-Elasticity* (Cambridge University Press, Cambridge, 1931).
28. M. M. Frocht, *Photoelasticity*, Vol. I and II (John Wiley & Sons, New York, 1948).
29. L. D. Landau and E. M.Lifchitz, *Theory of Elasticity*, revised and enlarged by E. M. Lifchitz, A. M. Kosevich and L. P. Pitaevskii (Butterworth-Heinemann, Oxford, 1997).

30. R. Dandliker, Rotational Effects of Polarization in Optical Fibres, in *Anisotropic and Non-linear Optical Waveguides*, C. G. Someda and G. Stegman, Eds. (Elsevier, Amsterdam, 1992).
31. J. Limeres, M. L. Calvo, V. Lakshminarayanan and J. M. Enoch, *J. Opt. Soc. Am.* B **20**, 1542 (2003).
32. S. R. Norman, D. N. Payne, M. J. Adams and A. M. Smith, *Electron. Lett.* **15**, 309 (1979).
33. V. Ramaswamy, W. G. French and R. D. Stanley, *Appl. Opt.* **17**, 3014 (1978).
34. I. P. Kaminow and V. Ramaswamy, *Appl. Phys. Lett.* **34**, 268 (1979).
35. R. H. Stolen, V. Ramaswamy, P. Kaiser and W. Pleibel, *Appl. Phys. Lett.* **33**, 699 (1978).
36. T. R. Wolinski, Polarimetric Optical Fibres and Sensors in *Progress in Optics*, Vol. XL, E. Wolf, Ed. (Elsevier, Amsterdam, 2000).
37. K. T. V. Grattan and T. Sun, *Sensors Actuators* **82**, 40 (200).
38. R. F. Cordero Ianarella, *J. Opt. Soc. Am.* **70**, 799 (1980).
39. R. L. Sidman, *J. Biophys. Biochem. Cytol.* **3**, 15 (1957).
40. D. E. Freund, R. L. McCally and R. A. Farrell, *Appl. Opt.* **25**, 2739 (1986).
41. T. B. Smith, *J. Mod. Opt.* **35**, 93 (1988).
42. G. J. Van Brokland and S. C. Verhelst, *J. Opt. Soc. Am.* A **4**, 82 (1987).
43. A. Sommer, H. A. Kues, S. A. D'Anna, S. Arkell, A. Robin and H. A. Quigley, *Arch. Ophthalmol.* **102**, 864 (1984).
44. A. Plesch, V. Klingbell and J. Bille, *Appl. Opt.* **26**, 1480 (1987).
45. A. W. Dreher, K. Reiter and R. N. Weinreb, *Appl. Opt.* **31**, 3730 (1992).
46. A. M. Benoit, K. Naoun, V. Louis-Dorr, L. Mala and A. Raspiller, *Appl. Opt.* **40**, 565 (2001).
47. B. R. Horowitz, Theoretical Considerations of the Retinal Photoreceptor as a Waveguide, in *Vertebrate Photoreceptor Optics*, J.M. Enoch and F.L. Tobey, Eds. (Springer-Verlag, Berlin, 1981).
48. P. A. Liebman, Birefringence, Dichroism and Rod Outer Segment Structure, in *Photoreceptor Optics*, A. W. Snyder and R. Menzel, Eds. (Springer-Verlag, Berlin, 1975).
49. V. Lakshminarayanan, J. E. Bailey and J. M. Enoch, *Optom. Vision Sci.* **74**, 1011 (1997).
50. S. Choi, M. Kono and J. M. Enoch, Evidence for Transient Strains at the Optic Disk and Nerve in Myopia: I Stiles-Crawford Effect Studies Performed over Time, presented at the Annual Meeting of Association for Research in Vision and Ophthalmology, Fort Lauderdale, Florida, May, 5–10 (2002).
51. L. Mandel and E. Wolf, *Optical Coherence and Quantum Optics* (Cambridge University Press, Cambridge, 1995).
52. P. M. Morse and H. Feshbach, *Methods of Theoretical Physics*, Vol. II, Ch. 13 (McGraw-Hill, New York, 1953).
53. M. L. Calvo and A. Duran, *Il Nuovo Cimento* **29B**, 277 (1975).
54. R. G. Newton, *Scattering Theory of Waves and Particles*, 2nd. Ed. (Dover, New York, 2002).
55. M. Lax, *Rev. Mod. Phys.* **23**, 287 (1951).
56. M. L. Goldberger and K. M. Watson, *Collision Theory* (Dover, New York, 2004).
57. M. L. Calvo and A. Duran, *Il Nuovo Cimento* **45B**, 68 (1978).
58. M. Abramowitz and I. A. Stegun, Eds. *Handbook of Mathematical Functions* (Dover, New York, 1955).
59. J. W. Goodman, *Introduction to Fourier Optics*, 2nd Ed. (McGraw-Hill, New York, 1996).

60. R. Barakat, *J. Opt. Soc. Am.* **54**, 921 (1964).
61. D. R. Williams and N. J. Coletta, *J. Opt. Soc. Am.* A **4**, 1514 (1987).
62. J. Limeres, M. L. Calvo, V. Lakshminarayanan and J. M. Enoch, Stress Sensor Based on Light Scattering by an Array of Birefringent Optical Waveguides in *International Commission for Optics XIX: Optics for the Quality of Life*, A. Consortini and G. C. Righini, Eds. *Proc. SPIE*, **4829**, 881 (2002).
63. M. L. Calvo and R. F. Alvarez-Estrada, Coupling of Dielectric Waveguide in *Max Born Centenary Conference*, M. J. Colles and D. Swift, Eds. *Proc. SPIE*, **369**, 401 (1982).
64. J. M. Enoch, S. S. Choi, M. Kono, V. Lakshminarayanan and M. L. Calvo, Receptor Alignments and Visual Fields in *High and Low Myopia*, Proceedings of Halifax Conference, September (2000).
65. R. F. Alvarez-Estrada and M. L. Calvo, *J. Math. Phys.* **21**, 389 (1980).